Article

Immunity

Loss of CD4+ T cell-intrinsic arginase 1 accelerates Th1 response kinetics and reduces lung pathology during influenza infection

Graphical abstract

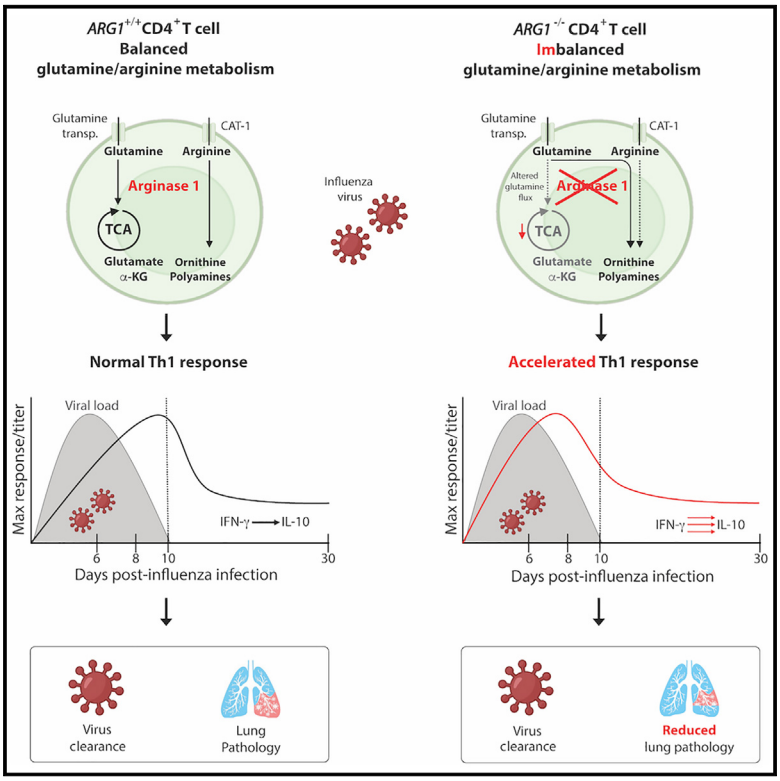

Highlights

- CD4+ T cell-intrinsic arginase 1 controls Th1 induction and contraction kinetics
- Loss of arginase 1 in CD4+ T cells results in reduced Th1-mediated tissue pathology
- Th1-intrinsic arginase 1 ensures balanced glutamine vs. arginine metabolism
- CD4+ T cell-intrinsic arginase 1 and 2 have distinct, non-overlapping functions

Authors

Erin E. West, Nicolas S. Merle, Marcin M. Kamiński, ..., Daniela Karall, Martina Huemer, Claudia Kemper

Correspondence

erin.west@nih.gov (E.E.W.), claudia.kemper@nih.gov (C.K.)

In brief

West et al. demonstrate that CD4+ T cell-intrinsic arginase 1 paces the transition of Th1 cells from their induction to their contraction program via balancing glutamine vs. arginine usage. They further show that Th1 cells lacking arginase 1 retain full pathogen clearance capacity but cause less Th1-associated tissue pathology.

West et al., 2023, Immunity *56*, 1–18
September 12, 2023 Published by Elsevier Inc.
https://doi.org/10.1016/j.immuni.2023.07.014

CellPress

Immunity

CellPress
OPEN ACCESS

Article

Loss of CD4+ T cell-intrinsic arginase 1 accelerates Th1 response kinetics and reduces lung pathology during influenza infection

Erin E. West,[1,*] Nicolas S. Merle,[1] Marcin M. Kamiński,[2] Gustavo Palacios,[2] Dhaneshwar Kumar,[3] Luopin Wang,[4] Jack A. Bibby,[1] Kirsten Overdahl,[5] Alan K. Jarmusch,[5] Simon Freeley,[6] Duck-Yeon Lee,[7] J. Will Thompson,[8] Zu-Xi Yu,[9] Naomi Taylor,[10,11] Marc Sitbon,[10,11] Douglas R. Green,[2] Andrea Bohrer,[12] Katrin D. Mayer-Barber,[12] Behdad Afzali,[3] Majid Kazemian,[4] Sabine Scholl-Buergi,[13] Daniela Karall,[13] Martina Huemer,[14,15,16] and Claudia Kemper[1,17,*]

[1]Complement and Inflammation Research Section (CIRS), National Heart, Lung, and Blood Institute (NHLBI), National Institutes of Health (NIH), Bethesda, MD, USA
[2]Department of Immunology, St. Jude Children's Research Hospital, Memphis, TN, USA
[3]Immunoregulation Section, Kidney Diseases Branch, National Institute of Diabetes and Digestive and Kidney Diseases (NIDDK), NIH, Bethesda, MD, USA
[4]Departments of Biochemistry and Computer Science, Purdue University, West Lafayette, IN, USA
[5]Immunity, Inflammation, and Disease Laboratory, Division of Intramural Research, National Institute of Environmental Health Sciences (NIEHS), NIH, Research Triangle Park, NC, USA
[6]School of Immunology and Microbial Sciences, King's College London, Guy's Hospital, Great Maze Pond, London SE1 9RT, UK
[7]Biochemistry Core, NHLBI, NIH, Bethesda, MD, USA
[8]Proteomics and Metabolomics Shared Resource, Center for Genomic and Computational Biology, Duke University, Durham, NC, USA
[9]Pathology Core, NHLBI, NIH, Bethesda, MD, USA
[10]Pediatric Oncology Branch, Rare Tumor Initiative, Center for Cancer Research, National Cancer Institute (NCI), NIH, Bethesda, MD, USA
[11]Institut de Génétique Moléculaire de Montpellier (IGMM), Université de Montpellier, CNRS, Montpellier, France
[12]Inflammation and Innate Immunity Unit, National Institute of Allergy and Infectious Diseases (NIAID), NIH, Bethesda, MD, USA
[13]Clinic for Pediatrics I, Inherited Metabolic Disorders, Medical University of Innsbruck, Innsbruck, Austria
[14]Division of Metabolism and Children's Research Center, University Children's Hospital Zurich, University of Zurich, Zurich, Switzerland
[15]Department of Pediatric Endocrinology and Diabetology, University Children's Hospital Basel, Basel, Switzerland
[16]Department of Pediatrics, Landeskrankenhaus (LKH) Bregenz, Bregenz, Austria
[17]Lead contact
*Correspondence: erin.west@nih.gov (E.E.W.), claudia.kemper@nih.gov (C.K.)
https://doi.org/10.1016/j.immuni.2023.07.014

SUMMARY

Arginase 1 (Arg1), the enzyme catalyzing the conversion of arginine to ornithine, is a hallmark of IL-10-producing immunoregulatory M2 macrophages. However, its expression in T cells is disputed. Here, we demonstrate that induction of *Arg1* expression is a key feature of lung CD4+ T cells during mouse *in vivo* influenza infection. Conditional ablation of *Arg1* in CD4+ T cells accelerated both virus-specific T helper 1 (Th1) effector responses and its resolution, resulting in efficient viral clearance and reduced lung pathology. Using unbiased transcriptomics and metabolomics, we found that *Arg1*-deficiency was distinct from *Arg2*-deficiency and caused altered glutamine metabolism. Rebalancing this perturbed glutamine flux normalized the cellular Th1 response. CD4+ T cells from rare *ARG1*-deficient patients or CRISPR-Cas9-mediated *ARG1*-deletion in healthy donor cells phenocopied the murine cellular phenotype. Collectively, CD4+ T cell-intrinsic Arg1 functions as an unexpected rheostat regulating the kinetics of the mammalian Th1 lifecycle with implications for Th1-associated tissue pathologies.

INTRODUCTION

The importance of interferon (IFN)-γ-producing CD4+ T helper 1 (Th1) cells for protective immunity to infections is undisputed. However, timely contraction of Th1 responses, which is characterized by reduced IFN-γ production and induction of the anti-inflammatory cytokine interleukin 10 (IL-10), is equally important to constrain Th1-driven tissue inflammation and permit tissue repair and a return to homeostasis.[1] This is exemplified by human diseases in which persistent Th1 inflammation majorly contributes to tissue injury, scarring, and loss of function, as seen in autoimmune settings such as inflammatory bowel disease, rheumatoid arthritis (RA) and multiple sclerosis,[2] and in infections, including coronavirus disease of 2019 (COVID-19).[3] The importance of timely Th1 contraction to limit detrimental tissue pathology is demonstrated in experimental mouse models, such as

Please cite this article in press as: West et al., Loss of CD4+ T cell-intrinsic arginase 1 accelerates Th1 response kinetics and reduces lung pathology during influenza infection, Immunity (2023), https://doi.org/10.1016/j.immuni.2023.07.014

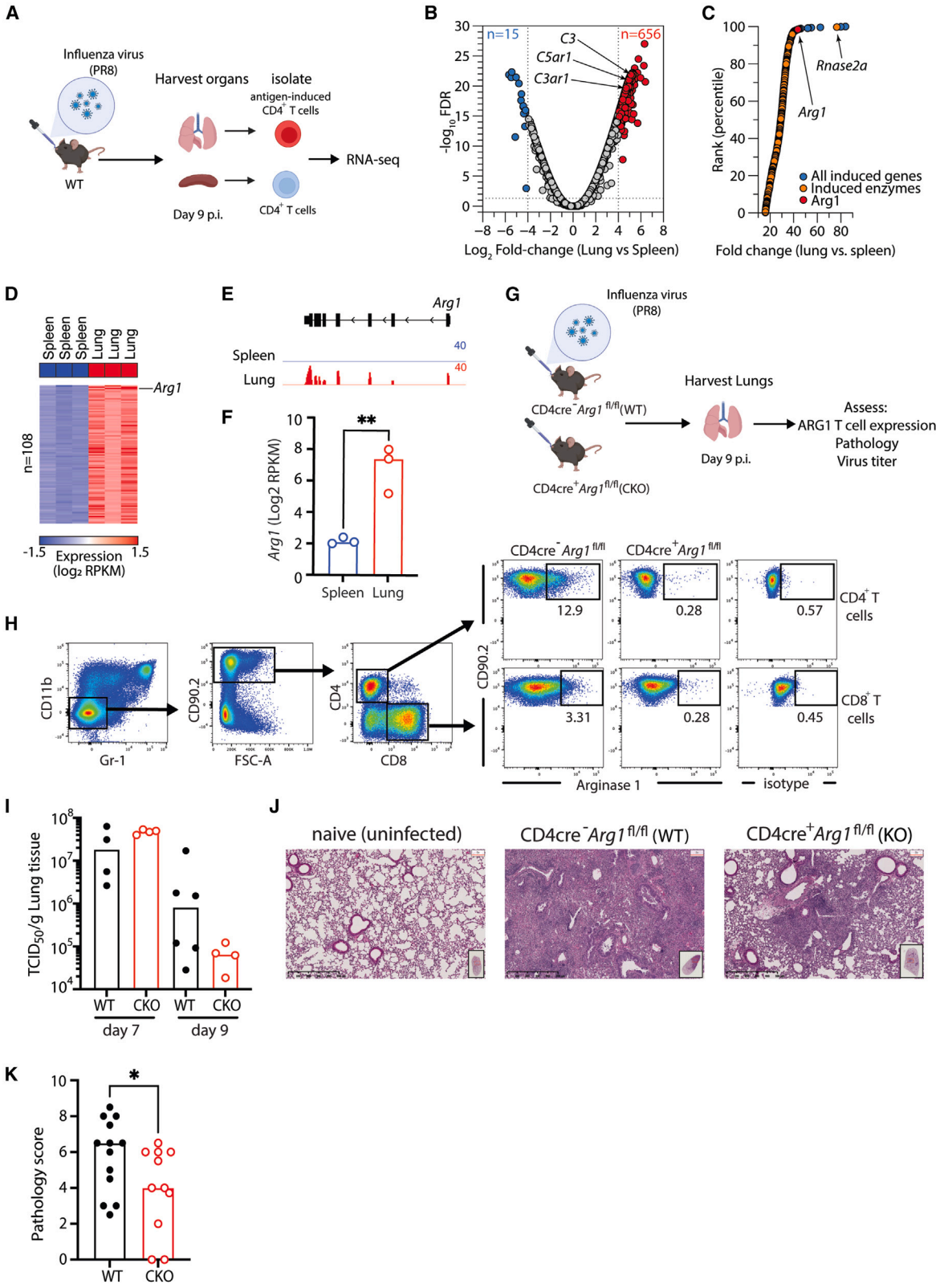

(legend on next page)

Please cite this article in press as: West et al., Loss of CD4+ T cell-intrinsic arginase 1 accelerates Th1 response kinetics and reduces lung pathology during influenza infection, Immunity (2023), https://doi.org/10.1016/j.immuni.2023.07.014

Toxoplasma gondii[1,4] and influenza virus infection,[5,6] in which antagonizing T cell-derived IL-10 enhances pathogen clearance but results in augmented tissue inflammation and lethal injury. Although it is broadly known that Th1 contraction is accompanied by metabolic reprogramming of the cells, only some changes are known, including increased cholesterol efflux and a reduction in glycolysis,[7–9] and the fine molecular details remain unelucidated.

To better understand the metabolic mechanisms underlying both Th1 initiation and cessation, we employed an influenza lung infection model where the CD4+ T cell response is Th1 dominated and encompasses both the Th1 induction and contraction phases, and where T cell IL-10 production is important for limiting lung pathology.[5] Here, in contrast to a previous report,[10] we identified expression of the enzyme arginase 1 (*Arg1*) by CD4+ T cells. ARG1 is an enzyme catalyzing conversion of arginine to ornithine and urea. By using mice with selective ablation of *Arg1* in T cells, CD4+ T cells from rare pediatric patients with ARG1-deficiency, and employing transcriptomic and metabolomic studies, we identified T cell-intrinsic ARG1 as a regulator of both human and mouse Th1 lifecycles: ARG1-deficient Th1 cells expand more rapidly and hasten toward IL-10-associated contraction. Biologically, this results in the efficient control of viral infection and reduced tissue inflammation and pathology post infection (p.i.). Mechanistically, normal ARG1 activity generates cell-essential ornithine from arginine and thereby ensures optimal glutamine flux into the tricarboxylic acid (TCA) cycle. In the absence of ARG1, compensatory utilization of glutamine for ornithine generation reduces TCA activity, which impacts the kinetics of the Th1 response. Overall, our data uncover a CD4+ T cell-intrinsic and non-redundant role for ARG1 in Th1 biology, which could potentially be harnessed to prevent or limit tissue pathology in Th1-driven disease states.

RESULTS

T cell-intrinsic ARG1 modulates tissue pathology during influenza infection

To investigate pathways and enzymes that regulate the course of the Th1 CD4+ T cell effector response in a system where tissue Th1 responses and IL-10 production are known to play a relevant role, we performed RNA sequencing (RNA-seq) on flow-sort-purified influenza-induced lung CD4+ T cells (CD11a+ CD49d+ TCRb+ CD4+) from wild-type (WT) mice infected with PR8, a pathogenic mouse-adapted strain of H1N1 influenza, and compared their RNA expression profile to splenic CD4+ T cells from these same mice (as a negative control, as splenic T cells are not enriched for an influenza-specific response) (Figure 1A). CD11a and CD49d are common surrogate markers of virus-induced and antigen-specific T cells in both mice and humans after viral infections or vaccination[11–16] and allow for the unbiased tracking of the broad CD4+ T cell response in the mouse lung after influenza exposure.[12]

656 and 15 genes showed increased and decreased expression, respectively, in lung CD4+ T cells upon infection. Among the most elevated genes in influenza-activated effector CD4+ T cells were those encoding components of the complement system, such as *C3*, *C5ar1*, and *C3ar1* (Figure 1B), consistent with previous findings that identified the induction of complement system genes as a central feature of protective T cell tissue immunity.[17] Unexpectedly, within the most highly induced genes (assessed by fold induction) was the enzyme *Arg1*, which ranked number 3 among all induced enzymes, after *Rnase2a* and *Pnpla5*, and which was the 11th most highly induced gene overall (top 1.5 percentile) (Figures 1C–1F; Table S1).

High induction and the prominent position in the hierarchy of induced genes indicated a probable role for cell-intrinsic *Arg1* in CD4+ T cells and virus-induced Th1 responses. We therefore generated mice with a conditional deletion of *Arg1* expression specifically in T cells using CD4cre (CD4cre+ *Arg1*$^{fl/fl}$, *Arg1* conditional knockout [CKO] mice) and repeated the PR8 infection experiment using these animals (Figure 1G). Both, CD4+ and CD8+ T cells from WT mice expressed ARG1 protein (with CD4+ T cells producing higher amounts compared to CD8+ T cells) and Cre-mediated *Arg1* deletion abrogated ARG1 production in both lineages, as expected[18] (Figures 1H and S1A). *Arg1* deletion was specific to CD4+ and CD8+ T cells, as CD11b+ macrophages/neutrophils retained ARG1 protein expression in *Arg1* CKO animals (Figure S1B). Upon influenza infection, WT and *Arg1* CKO mice cleared the virus similarly (Figure 1I). However, compared with WT mice, the *Arg1* CKO had a reduction in lung injury, evidenced by reduced inflammation (Figure 1J) and pathology score (Figure 1K) at day 9 p.i., indicating a role for T cell-intrinsic *Arg1* in regulating lung pathology during influenza infection.

CD4+ T cell ARG1 controls the kinetics of the Th1 influenza response

To further elucidate how T cell-intrinsic ARG1 influences *in vivo* CD4+ T cell responses, we infected WT and *Arg1* CKO mice with influenza PR8 and assessed the lung T cell responses at days 7 and 9 p.i. (Figure 2A). There were no differences in the total numbers of mononuclear lung cells between WT and *Arg1* CKO mice at any time point analyzed p.i. (Figure 2B). However,

Figure 1. T cell-intrinsic arginase 1 modulates tissue pathology during influenza infection

(A) Experimental setup for (A)–(F), n = 3 individual mice/group.

(B) Volcano plot from RNA-seq identifying differentially expressed genes (DEGs), with at least $\log_2$ 4-fold change at FDR < 0.05, between virus-induced lung and splenic CD4+ T cells.

(C) Induced genes from (B) ranked by fold induction.

(D) Heatmap of gene expression induction of all induced enzymes (orange) with *Arg1* position indicated (red).

(E and F) Representative (E) RNA-seq tracks of the *Arg1* locus and (F) *Arg1* expression (RNA-seq) in splenic and lung CD4+ T cells after influenza infection.

(G) Experimental setup for (H)–(K).

(H) Representative fluorescence-activated cell sorting (FACS) plots of ARG1 protein expression in WT and *Arg1* CKO mice.

(I) Viral titers in the lung at days 7 and 9 p.i. Representative experiment (of two independent experiments) shown with n = 4–5 mice per group per time point.

(J) Representative hematoxylin and eosin (H&E) histology staining and (K) pathology score of the lungs at day 9 p.i. Combined data from two independent experiments, n = 11–13. *p < 0.05 (two-tailed Student's t test). Each dot represents a sample from an individual mouse. See also Figure S1.

Please cite this article in press as: West et al., Loss of CD4+ T cell-intrinsic arginase 1 accelerates Th1 response kinetics and reduces lung pathology during influenza infection, Immunity (2023), https://doi.org/10.1016/j.immuni.2023.07.014

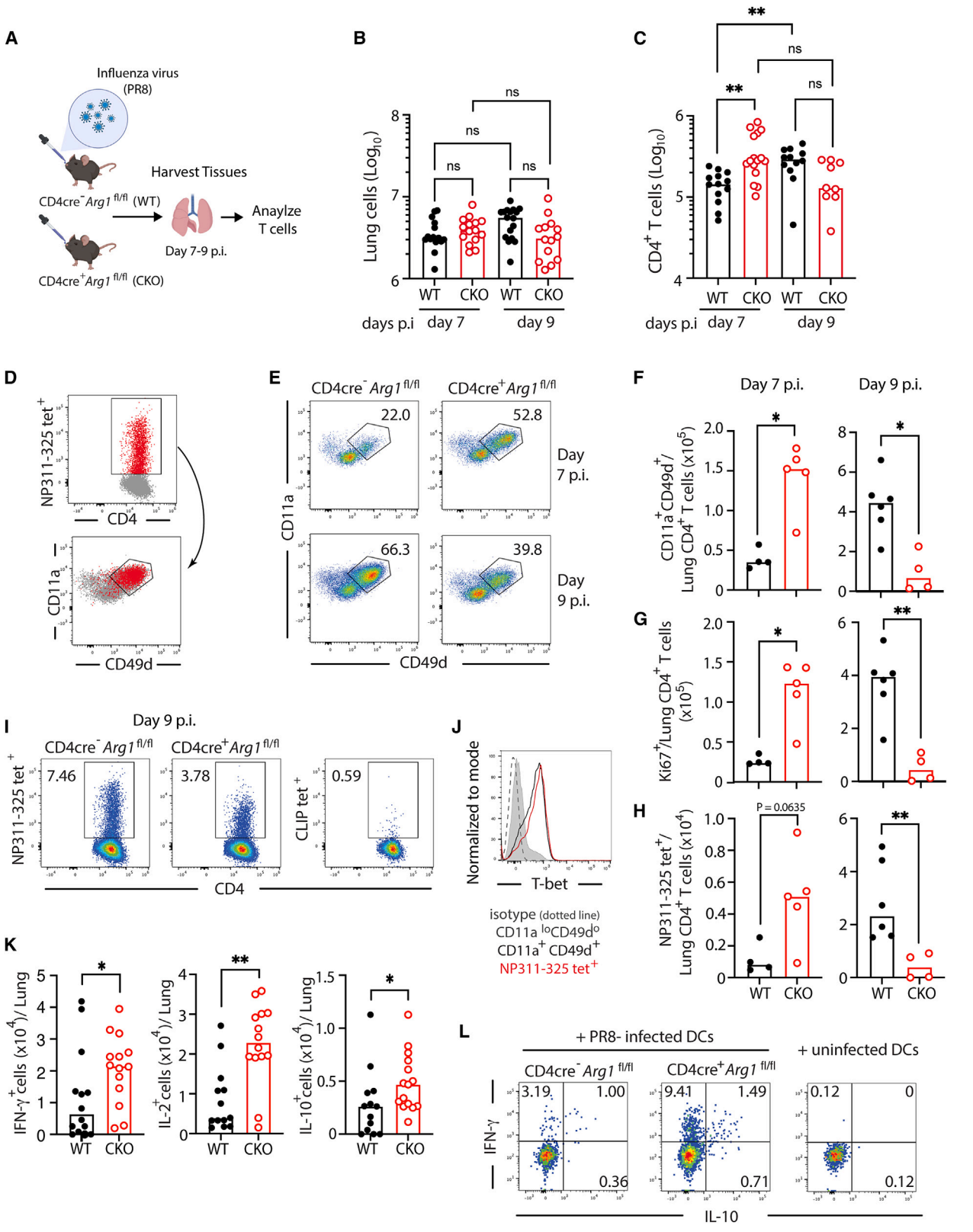

Figure 2. CD4+ T cell arginase 1 controls the kinetics of the Th1 influenza response

(A) Experimental setup for (B)–(L).

(B and C) Numbers of (B) total lung mononuclear cells and (C) lung CD4+ T cells at days 7 and 9 p.i., n = 12–17.

(legend continued on next page)

Please cite this article in press as: West et al., Loss of CD4+ T cell-intrinsic arginase 1 accelerates Th1 response kinetics and reduces lung pathology during influenza infection, Immunity (2023), https://doi.org/10.1016/j.immuni.2023.07.014

at day 7 of infection, we noted increased numbers of CD4+ T cells in the lungs of *Arg1* CKO mice when compared with WT mice (Figure 2C). Further, while the overall lung CD4+ T cell response increased, as expected, at day 9 p.i. in WT mice, CD4+ T cell numbers in *Arg1* CKO animals showed a trend toward decline at this time point (Figure 2C). These observations were fully recapitulated when we tracked lung CD11a+ CD49d+ CD4+ T cells, which encompass the broad (multi-epitope) influenza response, including the influenza-specific NP311-325 tetramer+ response (Figure 2D) at days 7 and 9 p.i. Early during infection (day 7), the lungs of *Arg1* CKO mice contained increased frequencies and numbers of virus-induced CD4+ T cells when compared with WT mice (Figures 2E and 2F, left). Additionally, the numbers of actively dividing Ki67+ CD4+ T cells were also higher in *Arg1* CKO mice (Figure 2G, left), indicating enhanced early proliferation by CD4+ T cells lacking *Arg1*. In contrast, at day 9 post infection, the frequencies and numbers of CD11a+ CD49d+ lung CD4+ T cells and dividing CD4+ T cells were reduced in the *Arg1* CKO compared with WT (Figures 2E–2G, right). The influenza-specific CD4+ NP311 tetramer+ cells mirrored the CD11a+ CD49d+ responses noted at days 7 and 9 in WT and *Arg1* KO mice (Figures 2H and 2I), in line with previous observations showing that lung CD11a+CD49d+ CD4+ T cells are indicative of the lung influenza-specific response.[12] T cell *Arg1*-deficiency did not alter the distribution of effector and memory phenotype cells within the influenza-induced and -specific CD4+ T cells (Figures S2A and S2B). Thus, the expansion of WT and *Arg1* CKO CD4+ T cells appears to follow different kinetics in response to influenza infection, with the latter exhibiting an earlier expansion and a faster subsequent contraction.

We next studied the cytokine production by CD4+ T cells following influenza infection. CD4+ T cell responses are typically dominated by Th1 responses during influenza infection,[19] and, indeed, both CD11a+ CD49d+ lung CD4+ T cells and the influenza-specific NP311 tetramer+ lung cells strongly expressed the Th1 transcription factor T-bet (Figures 2J and S2C). Additionally, we detected negligible IL-17A production from either WT or *Arg1* CKO CD4+ T cells (Figure S2D). However, when compared with WT CD4+ T cells, *Arg1* CKO CD4+ T cells from the lungs of mice at day 7 p.i. had higher frequencies and numbers of IFN-γ, IL-2, and tumor necrosis factor alpha (TNF-α)-producing cells, as well as IL-10-producing cells after *ex vivo* restimulation with influenza-infected dendritic cells (Figures 2K, 2L, S2E, and S2F), indicative of an enhanced early Th1 response.

CD8+ T cells are also *Arg1*-deficient in the CKO mice; we therefore assessed their CD8+ T cell response to influenza as well. *Arg1*-deficient CD8+ T lymphocytes (both total lung CD8+ T cells and CD11a+ CD49d+ CD8+ T cells) showed a trend toward augmented expansion at day 7 p.i., which did not reach statistical significance (Figures S2G and S2H). Although, we detected reduced numbers of total CD8+ T cells in the lungs of *Arg1* CKO mice at day 9 p.i., there was no difference in the number of influenza-induced CD11a+ CD49+ CD8+ T cells (Figures S2G and S2H). Furthermore, the key CD8+ T cell effector functions, IFN-γ production and cytotoxic degranulation, remained unaffected in *Arg1* CKO CD8+ T cells after *ex vivo* restimulation with influenza-infected dendritic cells (Figure S2I). This suggests that *Arg1*-deficiency in CD8+ T cells has limited effects on their anti-viral effector responses during influenza infection.

Collectively, these data demonstrate that CD4+ T cells lacking *Arg1* display an accelerated progression through the Th1 lifecycle compared with WT CD4+ T cells: they proliferate more rapidly, produce Th1 cytokines earlier, and move faster into the contraction phase upon influenza infection. Biologically, accelerated Th1 induction translates into efficient virus control, whereas quicker contraction, including enhanced IL-10 production, protects against excessive tissue injury.[20]

CD4+ T cell-intrinsic ARG1 controls the kinetic response and tissue pathology

Because CD4cre+ *Arg1*fl/fl animals lack ARG1 expression in both CD4+ and CD8+ T cells, we set out to ensure the specific contribution of CD4+ T cell-intrinsic *Arg1* in the CD4+ T cell response and T cell-mediated tissue pathology. First, we determined that *Arg1* CKO CD4+ T cells and WT CD4+ T cells have similar homeostatic proliferation when transferred together into *Rag* KO mice (Figures 3A–3D). Next, to assess whether the accelerated influenza-induced CD4+ T cell response in *Arg1* CKO mice was due to loss of CD4+ T cell-intrinsic ARG1, we transferred congenically labeled WT and *Arg1* CKO CD4+ T cells along with WT CD8+ T cells into *Rag* KO mice and assessed their responses early during infection (Figure 3E). As seen with infection of the *Arg1* CKO mice at day 7 p.i., transferred *Arg1*-deficient CD4+ T cells had an increased frequency of virus-induced CD11a+ CD49d+ cells and increased proliferation (Figures 3F–3H). These data demonstrate that CD4+ T cell-intrinsic *Arg1* regulates the CD4+ T cell effector response during influenza infection, independently from contributions of ARG1 expressed by CD8+ T cells.

To pinpoint whether CD4+ T cell-intrinsic *Arg1* also modulates CD4+ T cell-driven tissue pathology, we used a CD4+ T cell transfer model of colitis in which pathology is typically driven by Th1 responses (IFN-γ responses).[21–23] Using this model, we observed that the transfer of sorted naive splenic CD4+ T cells (CD45RBhi CD25−CD4+ T cells) from *Arg1* CKO mice into *Rag1*-deficient recipients caused less colitis, including lower inflammation and overall reduction in the pathology severity score, compared with *Rag1*-deficient mice that had

(D and E) Representative FACS plots showing (D) influenza-specific (NP311-325 tetramer+) lung CD4+ T cells and their CD11a and CD49d expression (in red) and (E) percentages of lung CD11a+ CD49d+ cells.

(F–H) Numbers of lung (F) CD11a+ CD49d+ CD4+ T cells, (G) Ki67+ CD4+ T cells, and (H) NP311-235 tetramer+ CD4+ T cells at days 7 and 9 p.i. in WT and *Arg1* CKO mice, n = 4–6.

(I and J) Representative FACS plots of (I) lung NP311-235 tetramer+ CD4+ T cells and (J) T-bet expression by CD11alo CD49dlo, CD11a+CD49d+, and NP311-235 tetramer+ CD4+ T cells at day 9 p.i.

(K and L) Numbers of (K) intracellular IFN-γ+, IL-2+, and IL-10+-producing lung CD4+ T cells (at day 7 p.i. and after *in vitro* restimulation with PR8-infected or non-infected dendritic cells), with (L) a representative FACS plot of data in (K), n = 14–15. *p < 0.05, **p < 0.01.

(B and C) Kruskal-Wallis test; (F–I and L) Mann-Whitney test. ns, no statistically significant difference. (B, C, K, and L) Combined data from three individual experiments. (F–H) One representative of three independent experiments shown. Each dot represents a sample from an individual mouse. See also Figure S2.

Please cite this article in press as: West et al., Loss of CD4+ T cell-intrinsic arginase 1 accelerates Th1 response kinetics and reduces lung pathology during influenza infection, Immunity (2023), https://doi.org/10.1016/j.immuni.2023.07.014

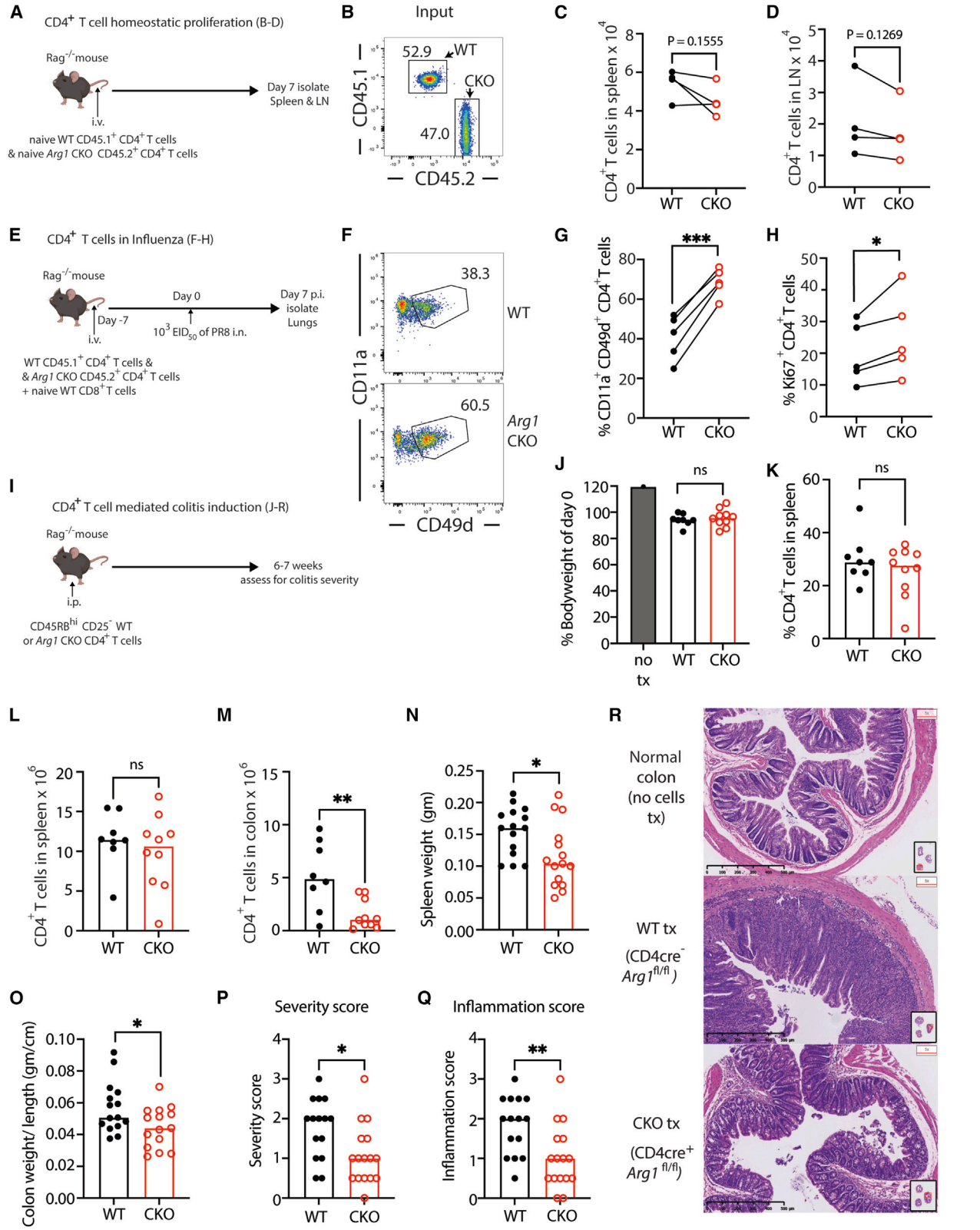

Figure 3. *Arg1* regulation of CD4+ T cell responses and pathology is CD4+ T cell-intrinsic

(A) Experimental setup for (B)–(D).

(B) Representative FACS plot showing transferred WT and *Arg1* CKO CD4+ T cells.

(legend continued on next page)

received WT CD4+ T cells (Figures 3I–3R). Taken together, these data demonstrate that CD4+ T cell-intrinsic *Arg1* regulates Th1 cell effector responses, including the tissue pathology associated with these responses.

Intrinsic ARG1- but not ARG2-deficiency alters the Th1 life cycle

We next performed a series of *in vitro* experiments with CD4+ T cells isolated from the spleens of naive *Arg1* CKO and WT mice (Figure 4A). We noted no significant differences in T cell thymic development (albeit a slight increase in DN4 cells in *Arg1* CKO mice (Figure S3A) or frequencies of naive and memory splenic CD4+ T cells (Figures 4B and S3B) between *Arg1* CKO and WT mice. In line with the changes observed in *in vivo*-elicited lung anti-virus CD4+ T cell responses (Figures 2C–2I), CD4+ T cells lacking *Arg1* exhibited a more pronounced early proliferation following *in vitro* CD3+CD28 activation (days 2.5–3, Figures 4C–4E, left), with reduced proliferation at later phases (day 5, Figure 4E, right) when compared with WT CD4+ T cells, while cell death remained unaffected (Figures S3C and S3D). Similarly, Th1 responses were also augmented in the *Arg1* CKO T cells, including a trend toward increased IFN-γ production and higher IL-10 induction compared with WT CD4+ T cells (Figures 4F, 4G, and S3E), broadly in agreement with our *in vivo* observations (Figures 2K and 2L). In contrast, the production of IL-17A, IL-5, IL-13, and IL-4 was not altered upon *in vitro* activation of *Arg1* CKO CD4+ T cells (Figures S3F–S3I). Additionally, *Arg1* CKO CD4+ T cells activated *in vitro* under Th1 polarizing conditions had enhanced IL-10 responses and increased proliferation with faster contraction (less proliferation at day 5 after activation) (Figures S3J–S3M), in line with our data under non-polarizing conditions (Figures 4C–4G). We noted no alterations in the frequency of FoxP3+ regulatory CD4+ T cells in the spleen, lymph nodes, or blood of *Arg1* CKO mice (Figures S3N and S3O), further supporting a specific role for ARG1 in Th1 type responses.

Arginase exists in two isoforms, ARG1 and arginase 2 (ARG2), with comparable enzymatic activities, but distinct preferences in tissue and subcellular location.[24] While ARG1 is mostly found in the cytoplasm, ARG2 accumulates in the mitochondria[25] (Figure 4H). Although ARG1 activity in T cells has thus far not been described, T cell-intrinsic ARG2 plays a role in regulating intracellular arginine concentrations, regulatory T cell numbers and function, and CD8+ T cell anti-tumor responses.[10,26,27] Thus, we next assessed the effect of *Arg2*-deficiency in CD4+ T cells on cytokine production. Naive *Arg2* KO mice exhibited decreased frequencies of naive ($CD44^{lo}$ $CD62L^{hi}$) and increased effector/effector memory ($CD44^{hi}$ $CD62L^{lo}$) CD4+ T cells in their spleens compared with WT mice (Figures 4I and S3B), in alignment with previous work reporting that ARG2 restrains CD8+ T cell memory development.[26] It is not possible to conclusively determine whether this is a CD4+ T cell-intrinsic *Arg2* effect because we utilized T cells from global *Arg2*-deficient animals. However, isolated *Arg2* KO CD4+ T cells displayed no significant difference in IFN-γ and IL-10 production, compared with WT CD4+ T cells, following *in vitro* stimulation (Figure 4J). Instead, *Arg2* KO CD4+ T cells secreted more IL-17A (Figures 4K and S3G) as well as IL-5, IL-13, and IL-4 (Figures S3H and S3I), suggesting that ARG2 restricts Th17 and Th2 responses. RNA-seq analyses of *in vitro* CD3 and CD28-activated CD4+ T cells from WT, *Arg1* CKO, and *Arg2* KO mice confirmed that *Arg1* and *Arg2* KO CD4+ T cells showed transcriptionally distinct profiles. More genes were differentially expressed between *Arg1*-deficient and WT or *Arg2*-deficient CD4+ T cells than there were when comparing *Arg2*-deficent vs. WT cells (Figure 4L; Table S2). Further, genes differentially expressed in *Arg1* CKO cells were especially enriched in IFN-γ responses and other IFN-γ-associated (e.g., allograft rejection, inflammatory response) biological pathways (Figure 4M). Taken together, these data indicate that *Arg1* expressed in CD4+ T cells plays a non-redundant function in the regulation of the Th1 lifecycle in a manner that is distinct from the functions of *Arg2*.

ARG1-deficient CD4+ T cells produce polyamines but exhibit metabolic perturbations

ARG1 mediates the conversion of arginine into ornithine and urea. Ornithine is utilized by cells to generate polyamines (putrescine, spermidine, and spermine; Figure 5A), which are crucial in governing T cell proliferation and effector cell fate.[28–32] Thus, we hypothesized that *Arg1* CKO CD4+ T cells would have a reduced ability to generate ornithine and downstream polyamines. However, mass spectrometry analyses of splenic WT and *Arg1* CKO CD4+ T cells revealed that ornithine and polyamine levels were unaltered in *Arg1* CKO CD4+ T cells (Figures 5B and 5C). Arginine levels in the *Arg1* CKO T cells were also normal (Figure 5D), indicating that the observed changes in the *Arg1* CKO CD4+ T cell response were not due to intracellular arginine accumulation, which has previously been observed in *Arg2*-deficient T cells.[10] Nonetheless, upon *in vitro* activation, *Arg1* CKO CD4+ T cells were unable to reach the levels of oxidative phosphorylation (OXPHOS) observed in WT CD4+ T cells, as shown by reductions in basal and maximal

(C and D) Numbers of CD4+ T cells recovered from (C) spleens and (D) lymph nodes 7 days post transfer, n = 4.
(E) Experimental setup for (F)–(H).
(F) Representative FACS plot of lung WT and *Arg1* CKO $CD11a^+$ $CD49d^+$ cells at day 7 p.i.
(G and H) Frequency of lung (G) $CD11a^+$ $CD49d^+$ CD4+ T cells and (H) $Ki67^+$ CD4+ T cells at day 7 p.i., n = 5.
(I) Experimental setup for (J)–(R).
(J) Body weight of mice receiving no cells, n = 1, or WT or *Arg1* CKO cells, n = 8–10.
(K) Percentage of CD4+ T cells in the spleens, n = 8–10.
(L and M) Numbers of CD4+ T cells in (L) spleens and (M) colons, n = 8–10. Representative of two individual experiments.
(N and O) Weight of (N) spleens and (O) colons of mice injected with WT or *Arg1* CKO CD4+ T cells, n = 15.
(P–R) Colon pathology of mice injected with WT or *Arg1* CKO based on (P) severity and (Q) inflammation, assessed via H&E histology staining. (R) Representative H&E staining of the colons.
(N–Q) Combined data from two individual experiments, n = 15 individual mice/group. Each dot represents a sample from a single mouse. *$p < 0.05$, **$p < 0.01$, ***$p < 0.001$. (C, D, G, and H) paired Student's t test; (J–Q) two-tailed Student's t test.

Please cite this article in press as: West et al., Loss of CD4+ T cell-intrinsic arginase 1 accelerates Th1 response kinetics and reduces lung pathology during influenza infection, Immunity (2023), https://doi.org/10.1016/j.immuni.2023.07.014

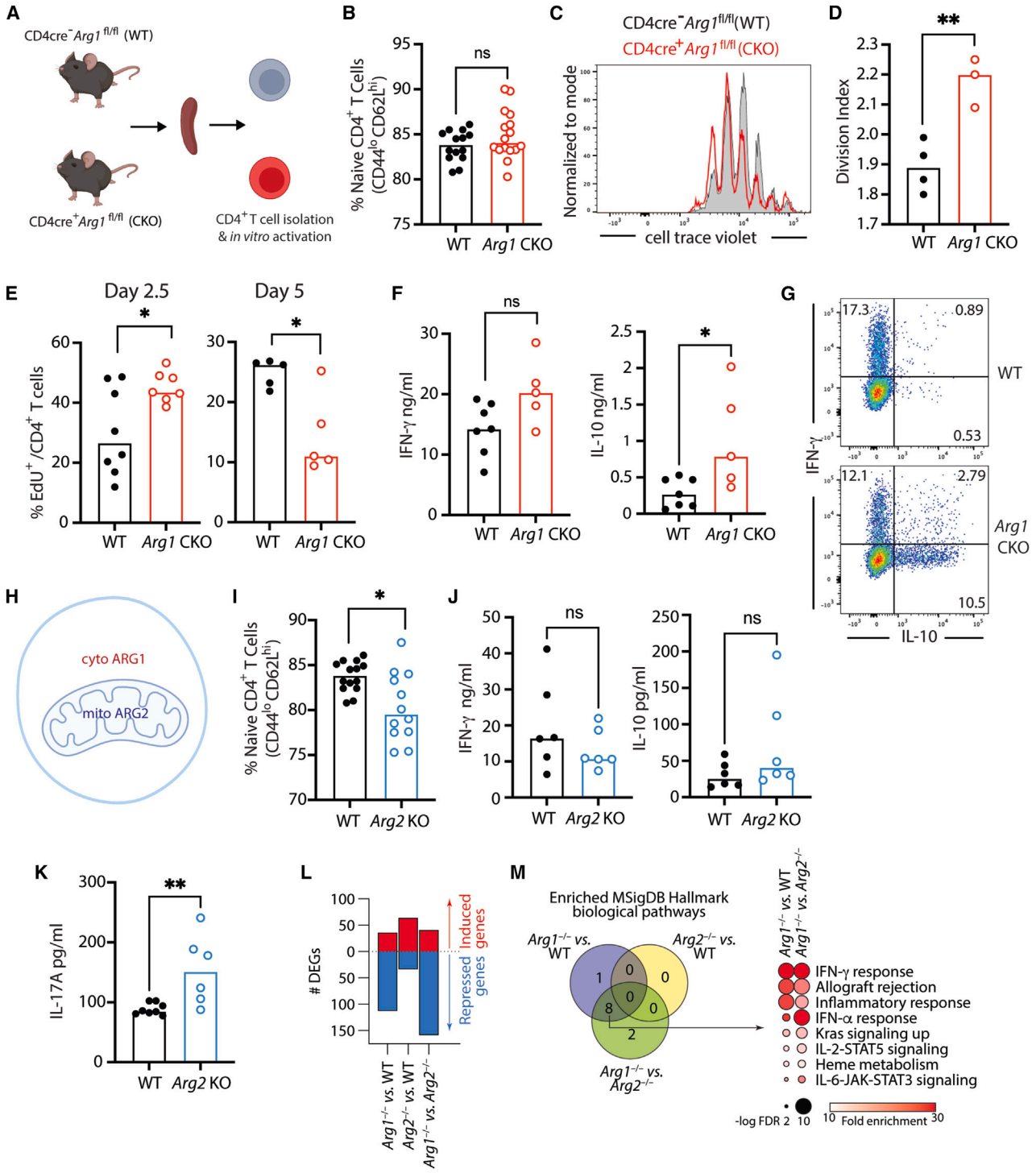

Figure 4. Intrinsic arginase 1, but not arginase 2, deficiency alters the Th1 life cycle

(A) Experimental setup for (B)–(G).

(B) Splenic naive CD4+ T cells in uninfected WT and *Arg1* CKO animals, n = 14–16 (data from four combined experiments shown).

(C and D) Representative (C) histogram of cell trace violet dilution at day 3 post activation and (D) division index (n = 3–4, one representative of two individual experiments shown).

(E) 5-ethynyl-2′-deoxyuridine (EdU) incorporation at days 2.5 (n = 7–8) and 5 (n = 5) post activation (data from two combined individual experiments).

(F) IFN-γ and IL-10 secretion at day 3 post activation (n = 5–7, data from two combined individual experiments shown).

(G) Representative FACS plots showing intracellular IFN-γ and IL-10 staining at 5 days post activation.

(H) Simplified schematic of ARG1 and ARG2 subcellular localization to cytoplasm (cyto) or mitochondria (mito).

(legend continued on next page)

Please cite this article in press as: West et al., Loss of CD4+ T cell-intrinsic arginase 1 accelerates Th1 response kinetics and reduces lung pathology during influenza infection, Immunity (2023), https://doi.org/10.1016/j.immuni.2023.07.014

oxygen consumption rates (OCRs), as well as spare respiratory capacity (Figures 5E and 5F). Further, *Arg1* CKO CD4+ T cells trended toward a reduction in glycolysis upon *in vitro* activation (Figures 5E and 5G) and these perturbations occurred despite the ability of *Arg1*-deficient CD4+ T cells to uptake glucose and activate mammalian target of rapamycin (mTOR) normally (Figures S4A and S4B). Hence, CD4+ T cells lacking ARG1 can unexpectedly generate ornithine and polyamines, but have perturbations in normal cell metabolism upon activation.

ARG1-deficiency in CD4+ T cells triggers altered glutamine metabolism

To better understand the cause of the metabolic differences between *Arg1* CKO and WT CD4+ T cells, we performed unbiased, untargeted, metabolomics on *Arg1* CKO and WT CD4+ T cells after *in vitro* activation. We identified glutamine as one of the metabolites most differentially abundant between *Arg1* CKO and WT CD4+ T cells, with glutamine levels strongly reduced in *Arg1* CKO CD4+ T cells (Figures 6A and 6B; Table S3). This was an intriguing finding because, in addition to feeding the TCA cycle in T cells via glutaminolysis to glutamate (Figure 6C), glutamine can also be utilized to generate ornithine and polyamines (Figure 6C)[28,33] and is particularly important during Th1 induction (Figure 6C).[28,33,34] Thus, we explored the possibility that a proportion of glutamine may be shunted from anaplerosis into ornithine and polyamine production in CD4+ T cells lacking *Arg1* expression. Indeed, although *Arg1 CKO* cells had normal glutamine uptake (Figure S5A), both glutamate and α-ketoglutarate (αKG), a TCA intermediate, were reduced in the *Arg1* CKO T cells (Figures 6D and 6E). Addition of a cell-permeable form of αKG (dimethyl-αKG [DM-KG]) reduced the accelerated *Arg1* CKO Th1 responses by normalizing their increased ratio of IL-10 vs. IFN-γ production (Figure S5B).

The idea that alterations in glutamine metabolism, here triggered by *Arg1*-deficiency, may contribute to the changes in Th1 responses observed in CD4cre+ *Arg1*$^{fl/fl}$ mice is consistent with a study suggesting that glutaminolysis restricts the Th1 response in mice.[35] Specifically, inhibition of glutamine synthase 1 (GLS1), a main enzyme converting glutamine to glutamate, by the inhibitor CB839 in CD4+ T cells (Figure S5C), results in increased *Ifng* gene transcription and Th1 induction. Mining these public data, we found evidence that a reduction in glutaminolysis (via CB839 treatment) also increased *Il10* gene transcription (Figure S6D, data derived from GEO: GSE112244). Thus, inhibition of normal glutamine metabolism likely alters both Th1 induction (IFN-γ) and contraction (IL-10) and phenocopies our observations made in *Arg1* CKO CD4+ T cells.

However, while a reduction of glutaminolysis aligns with the altered production of Th1 cytokines in the *Arg1* CKO CD4+ T cells, restriction of glutaminolysis is generally associated with a delay in early proliferation[35] and is contrary to the increased kinetic response exhibited by *Arg1* CKO CD4+ T cells. To understand this discrepancy, we took cues from what is known about the role of altered glutaminolysis in cancer cells. Cancer cells are highly proliferative and often dependent on glutamine. In fact, increased glutamine metabolism is now considered one hallmark of cancer.[36] Suppression of glutaminolysis, via inhibition of GLS, is therefore among the current methods being explored clinically to restrict cancer cell growth.[37–39] However, the induction of glutamic pyruvate transaminase 2 (GPT2), which catalyzes the reversible reaction between pyruvate and glutamate to generate alanine and αKG (Figure 6F), acts as a counter-measure to maintain TCA anaplerosis and cell growth in GLS-inhibited glutamine-dependent cancer cells.[40] Mining the previously published RNA-seq data from Johnson et al., we found evidence that CD4+ T cells express *Gpt2*. Further, reduced glutaminolysis, via inhibition of GLS1, resulted in increased *Gpt2* expression in Th1 cells (Figure S5E, data derived from GEO: GSE112244), suggesting that CD4+ T cells could compensate for reduced glutaminolysis by upregulating *Gpt2*. In line with this notion, we found that CD4+ T cells increased GPT2 protein upon activation (Figure S5F) and that *Arg1* CKO, but not *Arg2* KO CD4+ T cells, had a greater increase in GPT2 expression compared with WT cells (Figures 6G, 6H, S5F, and S5G). Further, inhibition of GLS (via treatment with CB839) or GPT2 inhibition (via treatment with the aminooxyacetate [AOA] transaminase inhibitor) resulted in aberrant intracellular glutamine and glutamate levels in CD4+ T cells, demonstrating the importance of these enzymes in glutamine metabolism in CD4+ T cells (Figures S5H–S5M). Importantly, GPT2 appears to play a role in CD4+ T cell proliferation, as inhibition of GPT2 (with AOA) during *in vitro* activation of CD4+ T cells dampens normal cell proliferation in a dose-dependent manner (Figures S5N and S5O). In addition, GPT2 inhibition in *Arg1* CKO CD4+ T cells normalized IL-10 levels without affecting IFN-γ production and rendered these cells now indistinguishable from WT CD4+ T cells (Figure 6I). Consistent with our findings that ARG2 may not play a role in Th1 responses, GPT2 inhibition had no effect on the *Arg2* KO CD4+ T cell IFN-γ or IL-10 production (Figure 6I).

Together, these data indicate that loss of ARG1 in CD4+ T cells results in altered glutamine metabolism/utilization and an adaptative increase in GPT2 expression, which may sustain cell proliferation in conjunction with increased IL-10 production (Th1 contraction).

ARG1 paces human Th1 responses and Th1 contraction

We next assessed whether our findings in mouse CD4+ T cells extend to human Th1 biology. Human Th1 induction and contraction requires the cell-intrinsic engagement of the human-specific co-stimulator CD46, a complement receptor, which supports nutrient influx and metabolic reprogramming during T cell activation.[7–9,41–43] *In vitro* activation of healthy human donor CD4+ T cells with antibodies to CD3 and CD46

(I) Splenic naive CD4+ T cells in naive WT and *Arg2* KO mice, n = 12–14 (data derived from four individual experiments).
(J and K) CD4+ T cells from WT and *Arg2* KO mice were activated *in vitro* for 3 days and (J) IFN-γ, IL-10, and (K) IL-17A measured (IFN-γ, n = 3; IL-10, n = 6, data from two combined individual experiments; IL-17A, n = 3–4).
(L and M) RNA-seq analyses of CD4+ T cells from WT, *Arg1* CKO, or global *Arg2* KO mice at 22 h post *in vitro* activation (n = 3 individual mice/group) with (L) numbers of differentially expressed genes (DEGs) and (M) venn diagram and list of overlapping enriched biological pathways derived from DEGs. Each dot represents a sample from a single mouse. *p < 0.05, **p < 0.01.
(D–F and I–K) Two-tailed Student's t test. ns, no statistically significant difference. See also Figure S3.

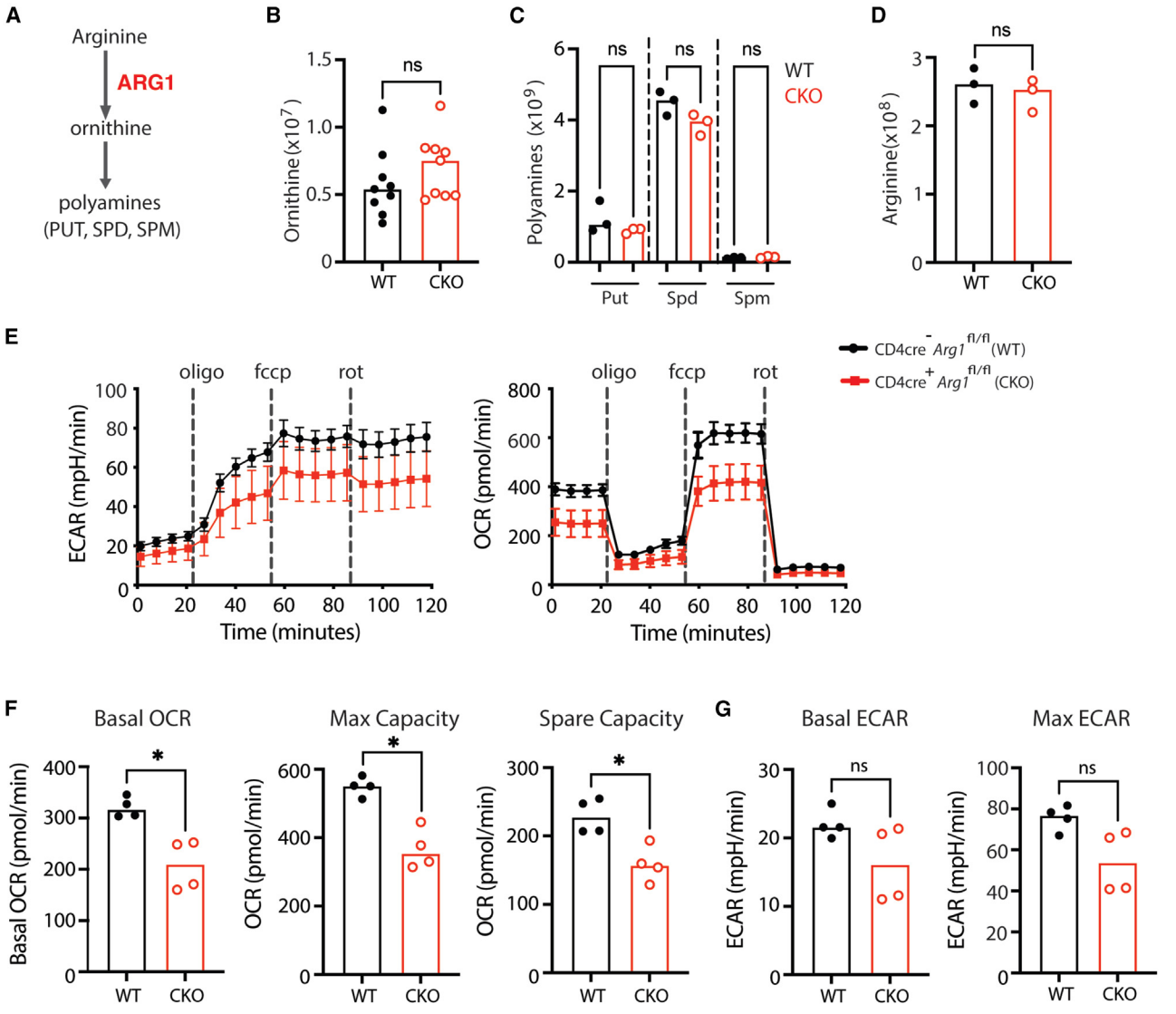

Figure 5. Arginase-1-deficient CD4+ T cells generate polyamines but have metabolic perturbations

(A) Simplified diagram of the classical arginase pathway.

(B–D) CD4+ T cells were isolated from the spleens of WT and *Arg1* CKO mice and stimulated *in vitro* with anti-CD3 and anti-CD28 antibodies for 22–24 h. (B) Ornithine, n = 3 samples from individual mice, done in triplicate; (C) polyamine, n = 3 samples from individual mice; and (D) arginine abundancy in the CD4+ T cells, as determined by liquid chromatography-mass spectrometry, n = 3 samples from individual mice.

(E–G) (E) Glycolysis (ECAR) and oxidative phosphorylation (OCR), as determined by Seahorse metabolomic profiling in response to oligomycin (oligo), carbonyl cyanide 4-(trifluoromethoxy) phenylhydrazone (fccp), and rotenone (rot) are shown with (F) accompanying statistical evaluation. ECAR, extracellular acidification rate; OCR, oxygen consumption rate. (E–G) n = 4, each dot represents individual mouse, one representative of three total experiments shown. *p < 0.05.

(B, D, F, and G) Mann-Whitney test; (C) Kruskal-Wallis test. ns, no statistically significant difference. See also Figure S4.

resulted in upregulation of ARG1 (Figures 7A and S6A) and accumulation of the main arginine transporter, cationic amino acid transporter 1/solute carrier family 7 member 1 (CAT-1/SLC7A1),[44] on the T cell surface (Figures 7B and S6B). Moreover, inhibition of arginases, *ARG1* and *ARG2*, via the pan arginase inhibitor Nω-hydroxy-nor-L-arginine (nor-NOHA) resulted in enhanced IFN-γ and IL-10 responses and an increase in the IL-10 to IFN-γ ratio (Figure 7C). These data suggest that T cell-intrinsic arginase may also play a regulative role in human Th1 biology. However, an isoform-specific inhibitor for ARG1, and not ARG2, is not available, and human CD4+ T cells do express ARG2 (Figure S6C). Thus, to address the specific effect of ARG1 absence we sourced blood samples from four rare pediatric patients with ARG1-deficiency (patients 1–4; Table S4) and analyzed their CD4+ T cell responses after *in vitro* activation in comparison with CD4+ T cell responses from age-matched healthy control (HC) individuals. ARG1-deficiency is an inherited disorder that leads to hyperammonemia and is associated with developmental delays, intellectual disabilities, seizures, and spasticity.[45] Importantly though, the immune cell phenotype of patients with ARG1-deficiency has thus far not been analyzed. We did not observe differences in the frequency of naive or

Please cite this article in press as: West et al., Loss of CD4+ T cell-intrinsic arginase 1 accelerates Th1 response kinetics and reduces lung pathology during influenza infection, Immunity (2023), https://doi.org/10.1016/j.immuni.2023.07.014

CellPress
OPEN ACCESS

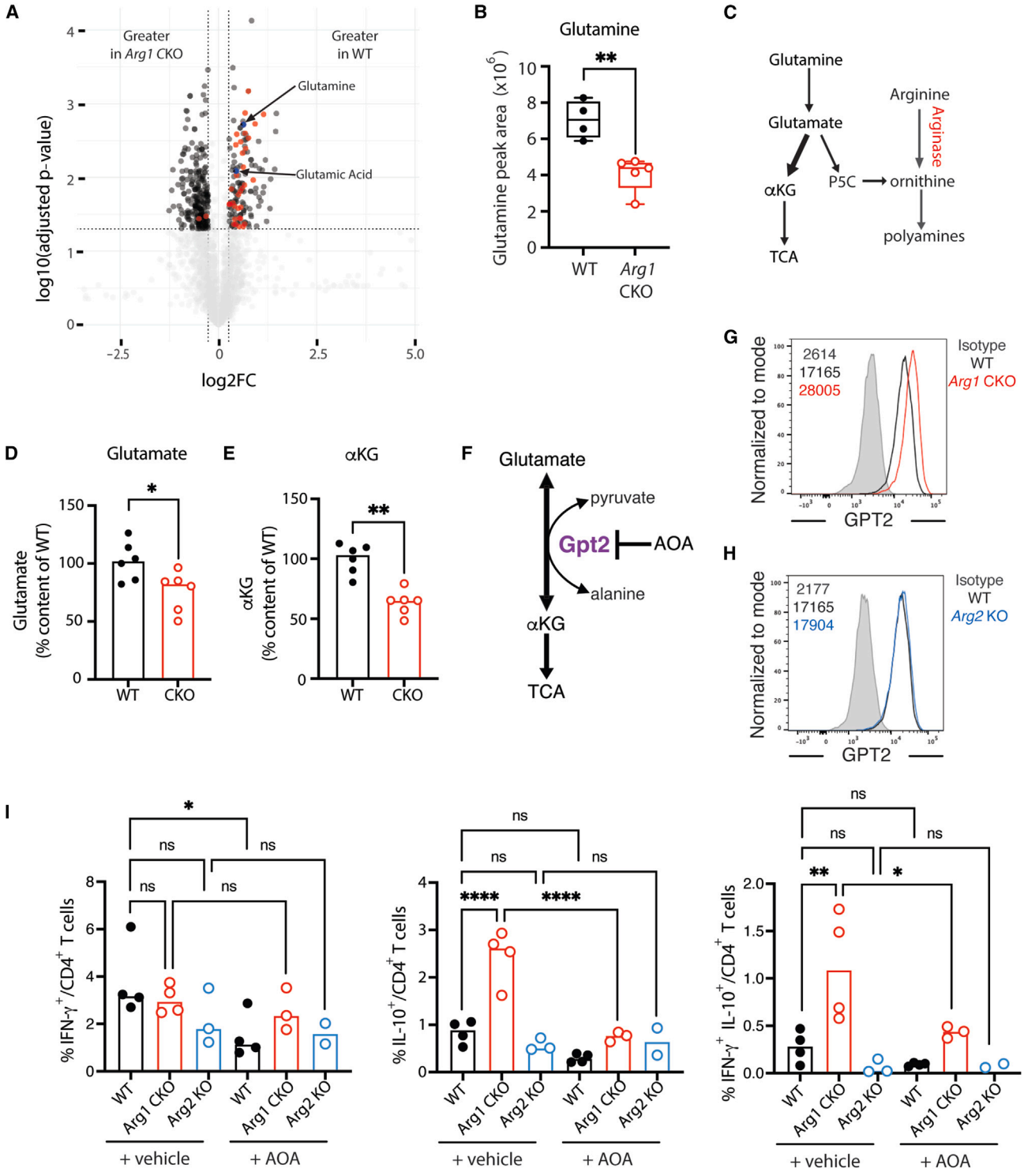

Figure 6. Arginase 1-deficiency in CD4+ T cells triggers altered glutamine metabolism

(A and B) Volcano plot of (A) differential metabolite abundance in *in vitro*-activated (22–24 h) CD4+ T cells from WT and *Arg1* CKO mice, n = 4–6. Positive and negative ionization mode features (gray), unannotated features that exceeded $log_2FC > 0.26$ (~20% change) and adjusted p value < 0.05 (black), annotated features which exceeded $log_2FC > 0.26$ and adjusted p value < 0.05 (red- and blue-highlighted and labeled for clarity), and (B) glutamine abundancy.

(C) Simplified schematic of intersecting arginine and glutamine pathways.

(D and E) Abundance of (D) glutamate and (E) α-ketoglutarate (αKG). For αKG, n = 3 individual mice shown with technical replicates.

(F) Schematic of *Gpt2* activity in glutamine metabolism.

(legend continued on next page)

Please cite this article in press as: West et al., Loss of CD4+ T cell-intrinsic arginase 1 accelerates Th1 response kinetics and reduces lung pathology during influenza infection, Immunity (2023), https://doi.org/10.1016/j.immuni.2023.07.014

memory CD4+ T cell populations between HCs and patients (Figure S6D). However, upon activation, the CD4+ T cells from patients produced IFN-γ within the normal range but displayed enhanced IL-10 production and hence an increased IL-10 to IFN-γ ratio compared with HC CD4+ T cells (Figures 7D and 7E). This skewing of Th1 cells toward IL-10 production in CD4+ T cells from patients with ARG1-deficiency was further amplified upon restimulation of CD4+ T cells (Figure 7F). IL-17 production was not affected in the patients' CD4+ T cells (Figure S6E), but we observed an increase in secretion of the Th1-associated cytokine TNF-α (Figure S6F). This indicated that loss of ARG1 in CD4+ T cells primarily affects Th1 responses in humans, congruent with the data observed in mouse *Arg1* CKO CD4+ T cells. Although we were unable to assess the proliferation of the patients' CD4+ T cells at an early time point due to the small blood sample volumes obtained, they exhibited decreased proliferative capacity at day 5 post activation as compared with HC CD4+ T cells (Figures 7G and 7H) and a reduction in the number of living cells upon restimulation (Figure 7I). The CD4+ T cells from the ARG1-deficient patients were able to uptake glutamine (Figure S6H) and contained normal amounts of polyamines (Figures 7J and S6G) but had less glutamine carbons incorporated into glutamate and into the TCA cycle intermediate, α-KG (Figures S6I–S6L). Further, they exhibited defective glycolysis and OXPHOS upon activation (Figure 7K), overall phenocopying the metabolic perturbations we saw in the *Arg1*-deficient mouse CD4+ T cells (we were unable to perform all experiments with CD4+ T cells from all of the patients due to low blood sample volume). Ablation of *ARG1* in HC CD4+ T cells by CRISPR-Cas9 also induced increased IL-10 switching/Th1 contraction (Figures S6M–S6O), without affecting IL-17A or IL-4 production (Figure S6P). In line with their cytokine production, the Th1-associated transcription factors, phospho-STAT-1 and STAT-4 and T-bet, were increased to similar levels in both the control and ARG1-depleted CD4+ T cells (Figures S6Q and S6R), demonstrating that *ARG1* ablation does not affect key regulators of Th1 function or identity. In addition, overexpression of ARG1 in healthy donor CD4+ T cells (Figure 7L) results in the opposite phenotype as *ARG1* depletion, with ARG1 overexpressing cells displaying normal IFN-γ production but decreased IL-10 production (Figures 7M and 7N) and a trend toward decreased proliferation (Figure 7O). Taken together, these data indicate that the altered Th1 responses in patients with ARG1-deficiency are not due to T cell developmental defects or their medication regimen.

The small volume of blood samples from the pediatric or young adolescent patients severely limits functional *ex vivo* experiments. To nonetheless obtain a broader overview of CD4+ T cell perturbations in these patients, we performed mRNA microarray and pathway analyses of anti-CD3 and CD46-activated T cells from two patients and age-matched controls. Ranked among the top pathways perturbed in the patients' CD4+ T cells were "metabolism of amino acids and derivatives" and "interleukin 10 signaling" (Figure 7P), lending further support to the finding that cell-intrinsic ARG1 represents an unexpected functional intersection between amino acid metabolism and the Th1 shutdown program. Cumulatively, these data indicate that CD4+ T cell-intrinsic ARG1 restrains early proliferative clonal expansion as well as the switch into the IL-10-producing contraction phase in both mice and humans.

DISCUSSION

In this study, we demonstrate that, contrary to previous reports, ARG1 is expressed by both mouse and human CD4+ T cells. Functionally, ARG1 serves as a pace keeper of Th1 induction and contraction by restraining early proliferative expansion and the timely switch into the IL-10-producing contraction phase. Further, changes in the ARG1-mediated temporal control of Th1 immunity have significant biological impact, as a lack of CD4+ T cell-intrinsic ARG1 expression allows for effective pathogen control while also substantially reducing Th1-mediated tissue pathology. This may explain why pediatric patients with deficiency in ARG1 do not suffer from recurrent infections.

Although the role of T cell-intrinsic *ARG2* has been previously explored, the expression of *ARG1* in T cells has been disputed, as a previous study failed to observe ARG1 in mouse and human CD4+ T cells.[10] Here, we demonstrate that ARG1 and ARG2 appear to play distinct and non-redundant roles in CD4+ T cell biology: ARG1 and ARG2 engage transcriptionally distinct signatures in CD4+ T cells upon activation, and CD4+ T cell-intrinsic ARG1 specifically controls Th1 responses while ARG2 appears to impact mostly on Th2 and Th17 cytokine production. It is not entirely surprising that the two arginase isoforms have distinct functions, as the isoforms show different preferential expression across tissues and cells,[46] reside in different subcellular locations,[47] and display subtle differences in kinetic behavior.[48]

CD4+ T cells normally show preferential usage of cellular arginine for polyamine generation and retain high levels of glutamine for optimal glutaminolysis early during activation.[10] This amino acid comsumption pattern is lost in *Arg1*-deficient CD4+ T cells, indicating that ARG1 activity allows for balanced arginine vs. glutamine metabolism during Th1 induction. Our data suggest that the adaptive usage of glutamine in *Arg1*-deficient CD4+ T cells, likely to sustain polyamine generation (Figure 5C), changes the generation of key glutaminolysis/TCA cycle metabolites, which have been previously connected with increased Th1 effector function (IFN-γ production).[35] Importantly, reduced glutaminolysis also expedited the switch of Th1 cells into IL-10 co-production and their contraction program. The finding that provision of α-KG to *Arg1*-deficient CD4+ T cells reduced IL-10 co-production aligns with previous data showing that α-KG inhibits the suppressive capacity of CD4+ T cells activated under regulatory T cell (Treg) polarizing conditions.[49]

(G and H) Representative FACS plots showing glutamate pyruvate transaminase 2 (GPT2) protein expression in WT, (G) *Arg1* KO, and (H) *Arg2* KO CD4+ T cells on day 3 post *in vitro* activation.

(I) Percentage of IFN-γ+, IL-10+, and IFN-γ-IL-10 double-positive T cells assessed via flow cytometry after *in vitro* stimulation with or without AOA treatment, n = 2–4 (representative of two independent experiments). *p < 0.05, **p < 0.01, ****p < 0.0001.

(B, D, E, G, and I) Two-tailed Student's t test; (L) one-way ANOVA. ns, no statistically significant difference, TCA cycle, tricarboxylic acid cycle. See also Figure S5.

Please cite this article in press as: West et al., Loss of CD4+ T cell-intrinsic arginase 1 accelerates Th1 response kinetics and reduces lung pathology during influenza infection, Immunity (2023), https://doi.org/10.1016/j.immuni.2023.07.014

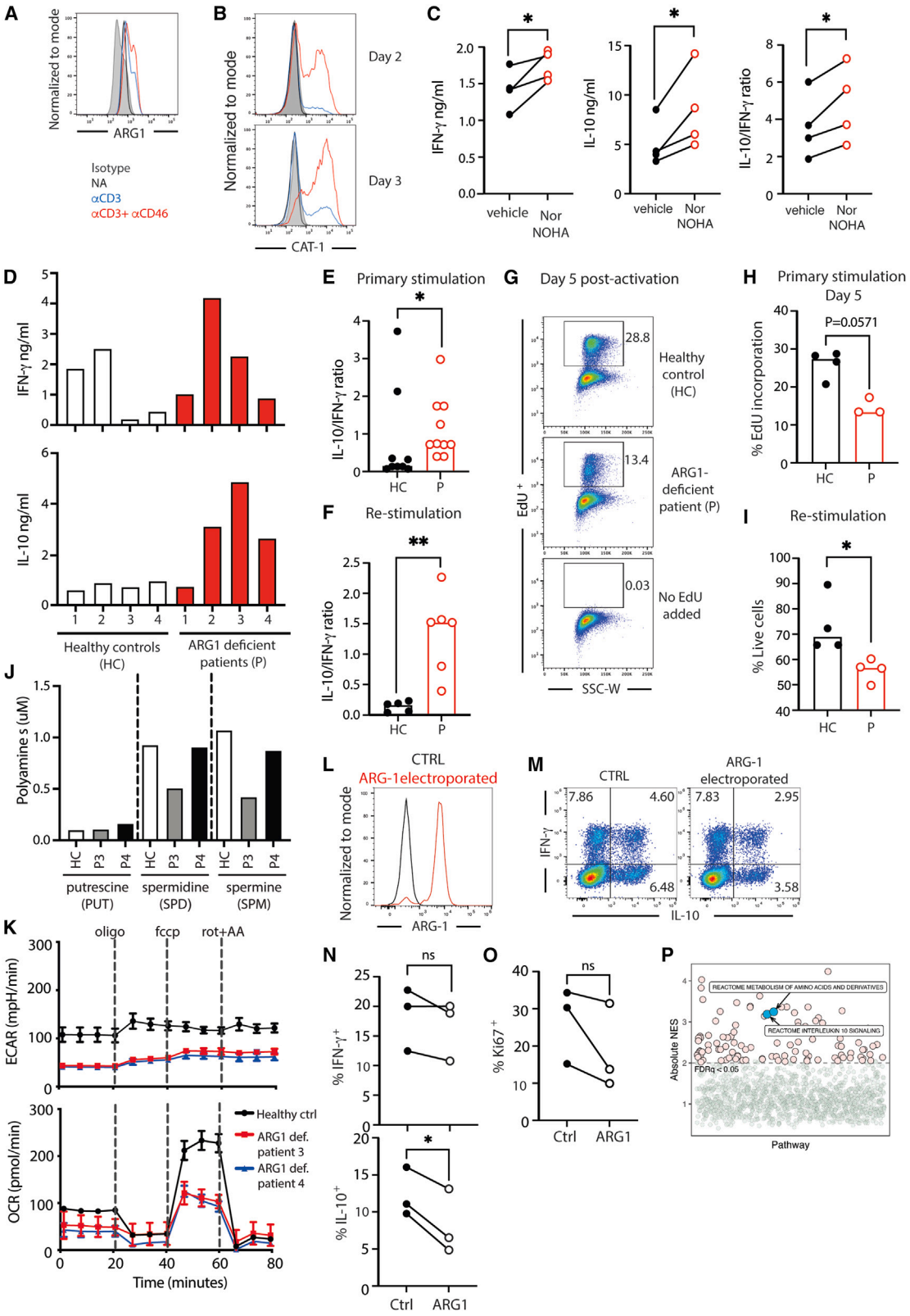

Figure 7. T cell-intrinsic arginase 1 restrains human Th1 responses and Th1 contraction

(A and B) Representative FACS plots showing (A) arginase 1 (ARG1) expression and (B) CAT-1 expression at days 2 and 3 in healthy donor CD4+ T cells after *in vitro* stimulation, n = 4.

(legend continued on next page)

Please cite this article in press as: West et al., Loss of CD4+ T cell-intrinsic arginase 1 accelerates Th1 response kinetics and reduces lung pathology during influenza infection, Immunity (2023), https://doi.org/10.1016/j.immuni.2023.07.014

The cross-regulative relationship between arginine and glutamine metabolism in CD4+ T cells described here is also potentially of interest to cancer biology. Altered glutamine metabolism (and often dependency) is a hallmark of cancer growth,[36] and inhibition/alteration of glutamine metabolism is an attractive metabolic therapy for cancer treatment.[50] In fact, we took cues from the cancer field to understand why *Arg1*-deficient CD4+ T cells proliferated so strongly despite reduced TCA cycle intermediates and reduced glycolysis: several cancer cells can adaptively upregulate GPT2, which catalyzes the reversible reaction between pyruvate and glutamate to produce alanine and proliferation supporting α-KG.[51] Indeed, *Arg1*-deficient CD4+ T cells seem to engage this adaptive rescue mechanism, as inhibition of GPT2 in *Arg1* CD4+ T cells normalized their Th1 response. Controlled GPT2 induction may also be part of the normal Th1 program, as inhibition of GPT2 reduced IFN-γ production and proliferation by CD4+ T cells isolated from WT mice (Figures 6I, S5N, and S5O). Thus, modulation of arginase/arginine metabolism could be a new avenue to explore in chimeric antigen receptor (CAR)-T cell biology.

A puzzling observation, however, remains the reduced glycolysis in CD4+ T cells lacking ARG1 expression, despite normal glucose uptake and S6 phosphorylation (Figure S4), and the acknowledged requirement of high glycolysis for Th1 induction.[52] We have previously shown that the return of glycolysis to near steady-state levels is associated with human Th1 contraction,[41] thus low glycolysis would principally align with the more rapid or increased IL-10 secretion observed by *Arg1* CD4+ T cells. Further, GPT2 is a pivot between glucose and glutamine metabolism and, as such, altered GPT2 levels will impact on important cell physiological pathways, including TCA activity, glucose carbon usage, mTORC1 activity, and autophagy—all pathways with known impact on T cell activation and effector programs.[53] Consequently, while the changes in glutamine metabolism in relationship to faulty ARG1 activity provide new explanations for altered Th1 kinetics, there are undoubtedly additional, undefined metabolic perturbations and adaptive responses engaged in *Arg1*-deficient CD4+ T cells.

Here, we observed that the accelerated Th1 life cycle was beneficial for the host and reduced Th1-associated tissue damage in an infection and intestinal autoimmune model, aligning well with previously reported data where IL-10 co-production by effector T cells drives the resolution of inflammation during influenza infections[5] and sustains mucosal tissue homeostasis.[54] However, in the context of other infectious diseases, such as *Leishmania major*,[55] *Listeria monocytogenes*,[56] and lymphocytic choriomeningitis virus (LCMV) infections,[57] excessive or prolonged IL-10 production by T cells is detrimental as it impedes effective pathogen clearance.[58] Although it is broadly recognized that timely Th1 contraction is required to prevent autoimmunity,[59] the exact effects of IL-10 co-induction by Th1 cells among the immune cell networks dysregulated in autoimmune states is still not fully delineated.[58] Therefore, *Arg1*-deficiency in CD4+ T cells may lead to different outcomes in other disease models.

Lastly, pharmacological modulation of ARG1 and ARG2 activity is becoming attractive for use as a medical intervention due to the association of pathological arginase expression with cancer progression, hypertension, and autoimmune, neurodegenerative, and cardiovascular disease.[60,61] However, another outcome of our work is the finding that ARG1 plays opposing roles in CD4+ T cells and in macrophages. Although ARG1 in CD4+ T cells sustains Th1 responses and contributes to tissue damage, in macrophages, ARG1 and ARG2 are markers of the anti-inflammatory M2 subtype and contribute to their IL-10 production and anti-inflammatory and tissue-repair capacities.[25,62,63] Thus, although ARG1 emerges as a therapeutic target of interest, we need to develop arginase-isoform-specific inhibitors, which currently do not exist,[61] and better understand the temporal and cell-specific activities of ARG1 across the immune cellular networks underlying different disease states.

Limitations of the study

Our data did not provide the exact molecular mechanism(s) by which Th1 cells sense changes in arginine and glutamine metabolism and translate those into the initiation of Th1 contraction, and tracing glutamine carbon incorporation into polyamines may help further shed light on this. Further, although we provide evidence as to why ARG1-deficient CD4+ T cells may still proliferate despite reduced glycolysis and OXPHOS via increased

(C) Amount of IFN-γ (left), IL-10 (middle), or ratio of IL-10 to IFN-γ (IL-10/IFN-γ) (right) secreted by CD4+ T cells after CD3+CD46 stimulation *in vitro* for 36 h in the presence of Nω-hydroxy-nor-L-arginine (nor-NOHA) or vehicle, n = 4.
(D–K) CD4+ T cells were isolated from the blood of patients with arginase-1 deficiency (designated as P) and age-matched healthy controls (designated as HC).
(D–F) IFN-γ and IL-10 secretion by CD3+CD46-activated CD4+ T cells (36 h, primary activation) with (D) individual values and (E) cumulative data for the IL-10/IFN-γ ratio during primary activation, n = 4 (four individual patients with multiple blood samples taken over a 2-year period), and (F) after CD3+CD46 restimulation for ~18–20 h post resting (5 days), n = 4 (individual patients, some with multiple blood samples taken over a 2-year period).
(G and H) 5-ethynyl-2′-deoxyuridine (EdU) incorporation at day 5 post primary stimulation with (G) a representative FACS plot and (H) cumulative data, n = 2 healthy controls with technical duplicates, and n = 3 patients.
(I) Percent of live CD4+ T cells after restimulation, as described under (F), n = 2 healthy controls done in duplicate and n = 3 patients, 1 with a technical duplicate.
(J) Polyamine abundancy in resting CD4+ T cells.
(K) Glycolysis (ECAR) and oxidative phosphorylation (OCR) as determined by Seahorse metabolomic profiling of CD4+ T cells after CD3+CD46 stimulation for 24 h.
(L–O) ARG1 was over expressed in isolated CD4+ T cells from three healthy donors (n = 3) by electroporation of ARG1 into the cells with (L) a representative FACS plot showing ARG1 expression in control (CTRL) electroporated versus ARG1 electroporated CD4+ T cells prior to activation. ARG1 overexpressing or control CD4+ T cells were activated *in vitro* for 36 h. (M) Representative FACS plot, (N) cumulative data showing IFN-γ and IL-10 production, and (O) percent of cells that are Ki67+.
(P) Pathway analysis of DEGs derived from microarray analyses of CD3+CD46-activated CD4+ T cells (6 h) from patients 1 and 2 and two age-matched healthy control cells, n = 2. *$p < 0.05$, **$p < 0.01$.
(C, N, and O) Paired Student's t test; (E, F, H, and I) Mann-Whitney test. fccp, carbonyl cyanide 4-(trifluoromethoxy) phenylhydrazone; ECAR, extracellular acidification rate; OCR, oxygen consumption rate; oligo, oligomycin; rot, rotenone. See also Figure S6 and Table S4.

GPT2 usage, their validation requires future experimental probing. Finally, we have only explored the phenotype of ARG1-deficiency in acute Th1 responses while its effect in recall responses, chronic infection, or other disease settings remains to be assessed.

STAR★METHODS

Detailed methods are provided in the online version of this paper and include the following:

- KEY RESOURCES TABLE
- RESOURCE AVAILABILITY
  - Lead contact
  - Materials availability
  - Data and code availability
- EXPERIMENTAL MODEL AND STUDY PARTICIPANT DETAILS
  - Healthy human donors and patients
  - Mice
- METHOD DETAILS
  - Antibodies, proteins and inhibitors
  - Mouse CD4$^+$ T cell isolation and activation
  - Mouse *in vitro* Th1 polarization
  - Human CD4$^+$ T cell isolation and activation
  - CD4$^+$ T cell proliferation assessment
  - Cytokine measurements
  - Glucose uptake and pS6 evaluation
  - OCR and ECAR measurements
  - Influenza infections, lung cell isolation and virus titers
  - Influenza cytokine assay
  - Influenza Lung Histology
  - CD4$^+$ T cell transfers into *Rag*$^{-/-}$ mice (homeostasis and CD4$^+$ T cell intrinsic influenza experiments).
  - Colitis induction and colon pathology scoring
  - CRISPR-Cas9 deletion of *ARG1*
  - ARG1 overexpression
  - Cell Preparations for Metabolomics
  - Untargeted Metabolomics
  - Extraction of hydrophilic metabolites for amino acid and polyamine measurement
  - Mouse amino acid and polyamine measurement
  - GC-MS-mediated analysis of TCA metabolites and ^{13}C-labelled TCA metabolites
  - Human polyamine measurement
  - RNAseq Library preparation and analysis
  - Microarray preparation and analysis
- QUANTIFICATION AND STATISTICAL ANALYSIS

SUPPLEMENTAL INFORMATION

Supplemental information can be found online at https://doi.org/10.1016/j.immuni.2023.07.014.

ACKNOWLEDGMENTS

We thank the patients and the healthy donors for their support, and Lisa St. John-Williams for technical assistance (metabolomics). The MHC class II tetramer to Influenza PR8 (NP311-325) was kindly provided by the NIH Tetramer Core. This work was financed by the National Heart, Lung, and Blood Institute of the NIH (grant 5K22HL125593 to M.K.), the Intramural Research Program of the NIH with support from the National Institute of Diabetes and Digestive and Kidney Diseases (project number ZIA/DK075149 to B.A.), the National Heart, Lung, and Blood Institute (project number ZIA/HL006223 to C.K.), and the Metabolomic Core of the National Institute of Environmental Health Sciences (project title "metabolic profiling of Th1 contraction" to E.E.W., Natalia Kunz, and C.K.).

AUTHOR CONTRIBUTIONS

Supervision, E.E.W., B.A., M.K., and C.K.; conceptualization, E.E.W. and C.K.; methodology, E.E.W., M.M.K., K.O., A.K.J., D.-Y.L., N.T., M.S., D.R.G., M.K., B.A., and C.K.; project administration, C.K.; investigation, E.E.W., N.S.M., M.M.K., G.P., D. Kumar, L.W., J.A.B., K.O., S.F., D.-Y.L., J.W.T., Z.-X.Y., K.D.M.-B., S.S.-B., D. Karall, and M.H.; formal analysis, E.E.W., N.S.M., M.M.K., D. Kumar, L.W., J.A.B., K.O., A.K.J., D.-Y.L., J.W.T., Z.-X.Y., N.T., M.S., K.D.M.-B., B.A., M.K., S.S.-B., D. Karall, M.H., and C.K.; resources, M.S., K.D.M.-B., A.B., S.S.-B., D. Karall, and M.H.; visualization, E.E.W., B.A., M.K., and C.K.; writing – original draft, E.E.W. and C.K.; funding acquisition, E.E.W. and C.K.

DECLARATION OF INTERESTS

M.S. is an inventor on a patent describing the use of RBD ligands for cell-surface evaluation of CAT1/solute carrier family 7 member 1 (SLC7A1) and other solute carrier (SLC) expression (N.T. gave up her rights); he is a co-founder and head of the scientific board of METAFORA-Biosystems, a start-up company that focuses on metabolite transporters under physiological and pathological conditions.

INCLUSION AND DIVERSITY

We support inclusive, diverse, and equitable conduct of research.

Received: October 14, 2022
Revised: June 1, 2023
Accepted: July 19, 2023
Published: August 11, 2023

REFERENCES

1. Jankovic, D., Kugler, D.G., and Sher, A. (2010). IL-10 production by CD4+ effector T cells: a mechanism for self-regulation. Mucosal Immunol. *3*, 239–246. https://doi.org/10.1038/mi.2010.8.
2. Khan, U., and Ghazanfar, H. (2018). T lymphocytes and autoimmunity. Int. Rev. Cell Mol. Biol. *341*, 125–168. https://doi.org/10.1016/bs.ircmb.2018.05.008.
3. Chauss, D., Freiwald, T., McGregor, R., Yan, B., Wang, L., Nova-Lamperti, E., Kumar, D., Zhang, Z., Teague, H., West, E.E., et al. (2022). Autocrine vitamin D signaling switches off pro-inflammatory programs of TH1 cells. Nat. Immunol. *23*, 62–74. https://doi.org/10.1038/s41590-021-01080-3.
4. Gazzinelli, R.T., Wysocka, M., Hieny, S., Scharton-Kersten, T., Cheever, A., Kühn, R., Müller, W., Trinchieri, G., and Sher, A. (1996). In the absence of endogenous IL-10, mice acutely infected with Toxoplasma gondii succumb to a lethal immune response dependent on CD4+ T cells and accompanied by overproduction of IL-12, IFN-gamma and TNF-alpha. J. Immunol. *157*, 798–805.
5. Sun, J., Madan, R., Karp, C.L., and Braciale, T.J. (2009). Effector T cells control lung inflammation during acute influenza virus infection by producing IL-10. Nat. Med. *15*, 277–284. https://doi.org/10.1038/nm.1929.
6. Arimori, Y., Nakamura, R., Yamada, H., Shibata, K., Maeda, N., Kase, T., and Yoshikai, Y. (2013). Type I interferon limits influenza virus-induced acute lung injury by regulation of excessive inflammation in mice. Antiviral Res. *99*, 230–237. https://doi.org/10.1016/j.antiviral.2013.05.007.
7. Cardone, J., Le Friec, G., Vantourout, P., Roberts, A., Fuchs, A., Jackson, I., Suddason, T., Lord, G., Atkinson, J.P., Cope, A., et al. (2010). Complement regulator CD46 temporally regulates cytokine production

by conventional and unconventional T cells. Nat. Immunol. *11*, 862–871. https://doi.org/10.1038/ni.1917.

8. West, E.E., Kolev, M., and Kemper, C. (2018). Complement and the regulation of T cell responses. Annu. Rev. Immunol. *36*, 309–338. https://doi.org/10.1146/annurev-immunol-042617-053245.
9. Perucha, E., Melchiotti, R., Bibby, J.A., Wu, W., Frederiksen, K.S., Roberts, C.A., Hall, Z., LeFriec, G., Robertson, K.A., Lavender, P., et al. (2019). The cholesterol biosynthesis pathway regulates IL-10 expression in human Th1 cells. Nat. Commun. *10*, 498. https://doi.org/10.1038/s41467-019-08332-9.
10. Geiger, R., Rieckmann, J.C., Wolf, T., Basso, C., Feng, Y., Fuhrer, T., Kogadeeva, M., Picotti, P., Meissner, F., Mann, M., et al. (2016). L-arginine modulates T cell metabolism and enhances survival and anti-tumor activity. Cell *167*, 829–842.e13. https://doi.org/10.1016/j.cell.2016.09.031.
11. Christiaansen, A.F., Dixit, U.G., Coler, R.N., Marie Beckmann, A., Reed, S.G., Winokur, P.L., Zimmerman, M.B., Varga, S.M., and Wilson, M.E. (2017). CD11a and CD49d enhance the detection of antigen-specific T cells following human vaccination. Vaccine *35*, 4255–4261. https://doi.org/10.1016/j.vaccine.2017.06.013.
12. Hornick, E.E., Zacharias, Z.R., and Legge, K.L. (2019). Kinetics and phenotype of the CD4 T cell response to influenza virus infections. Front. Immunol. *10*, 2351. https://doi.org/10.3389/fimmu.2019.02351.
13. McDermott, D.S., and Varga, S.M. (2011). Quantifying antigen-specific CD4 T cells during a viral infection: CD4 T cell responses are larger than we think. J. Immunol. *187*, 5568–5576. https://doi.org/10.4049/jimmunol.1102104.
14. Knudson, C.J., Weiss, K.A., Hartwig, S.M., and Varga, S.M. (2014). The pulmonary localization of virus-specific T lymphocytes is governed by the tissue tropism of infection. J. Virol. *88*, 9010–9016. https://doi.org/10.1128/JVI.00329-14.
15. Turner, D.L., and Farber, D.L. (2014). Mucosal resident memory CD4 T cells in protection and immunopathology. Front. Immunol. *5*, 331. https://doi.org/10.3389/fimmu.2014.00331.
16. Rai, D., Pham, N.L., Harty, J.T., and Badovinac, V.P. (2009). Tracking the total CD8 T cell response to infection reveals substantial discordance in magnitude and kinetics between inbred and outbred hosts. J. Immunol. *183*, 7672–7681. https://doi.org/10.4049/jimmunol.0902874.
17. Kolev, M., West, E.E., Kunz, N., Chauss, D., Moseman, E.A., Rahman, J., Freiwald, T., Balmer, M.L., Lötscher, J., Dimeloe, S., et al. (2020). Diapedesis-induced integrin signaling via LFA-1 facilitates tissue immunity by inducing intrinsic complement C3 expression in immune cells. Immunity *52*, 513–527.e8. https://doi.org/10.1016/j.immuni.2020.02.006.
18. Lee, P.P., Fitzpatrick, D.R., Beard, C., Jessup, H.K., Lehar, S., Makar, K.W., Pérez-Melgosa, M., Sweetser, M.T., Schlissel, M.S., Nguyen, S., et al. (2001). A critical role for Dnmt1 and DNA methylation in T cell development, function, and survival. Immunity *15*, 763–774. https://doi.org/10.1016/S1074-7613(01)00227-8.
19. Richards, K.A., Treanor, J.J., Nayak, J.L., and Sant, A.J. (2018). Overarching immunodominance patterns and substantial diversity in specificity and functionality in the circulating human influenza A and B virus-specific CD4+ T-cell repertoire. J. Infect. Dis. *218*, 1169–1174. https://doi.org/10.1093/infdis/jiy288.
20. Trinchieri, G. (2007). Interleukin-10 production by effector T cells: Th1 cells show self control. J. Exp. Med. *204*, 239–243. https://doi.org/10.1084/jem.20070104.
21. Powrie, F., Correa-Oliveira, R., Mauze, S., and Coffman, R.L. (1994). Regulatory interactions between CD45RB^{high} and CD45RB^{low} CD4+ T cells are important for the balance between protective and pathogenic cell-mediated immunity. J. Exp. Med. *179*, 589–600. https://doi.org/10.1084/jem.179.2.589.
22. Powrie, F., Leach, M.W., Mauze, S., Menon, S., Caddle, L.B., and Coffman, R.L. (1994). Inhibition of Th1 responses prevents inflammatory bowel disease in scid mice reconstituted with CD45RB^{hi} CD4+ T cells. Immunity *1*, 553–562. https://doi.org/10.1016/1074-7613(94)90045-0.
23. Kiesler, P., Fuss, I.J., and Strober, W. (2015). Experimental models of inflammatory bowel diseases. Cell. Mol. Gastroenterol. Hepatol. *1*, 154–170. https://doi.org/10.1016/j.jcmgh.2015.01.006.
24. Ash, D.E., Cox, J.D., and Christianson, D.W. (2000). Arginase: a binuclear manganese metalloenzyme. Met. Ions Biol. Syst. *37*, 407–428.
25. Dowling, J.K., Afzal, R., Gearing, L.J., Cervantes-Silva, M.P., Annett, S., Davis, G.M., De Santi, C., Assmann, N., Dettmer, K., Gough, D.J., et al. (2021). Mitochondrial arginase-2 is essential for IL-10 metabolic reprogramming of inflammatory macrophages. Nat. Commun. *12*, 1460. https://doi.org/10.1038/s41467-021-21617-2.
26. Martí i Líndez, A.A., Dunand-Sauthier, I., Conti, M., Gobet, F., Núñez, N., Hannich, J.T., Riezman, H., Geiger, R., Piersigilli, A., Hahn, K., et al. (2019). Mitochondrial arginase-2 is a cellautonomous regulator of CD8+ T cell function and antitumor efficacy. JCI Insight *4*, e132975. https://doi.org/10.1172/jci.insight.132975.
27. Lowe, M.M., Boothby, I., Clancy, S., Ahn, R.S., Liao, W., Nguyen, D.N., Schumann, K., Marson, A., Mahuron, K.M., Kingsbury, G.A., et al. (2019). Regulatory T cells use arginase 2 to enhance their metabolic fitness in tissues. JCI Insight *4*, e129756. https://doi.org/10.1172/jci.insight.129756.
28. Puleston, D.J., Baixauli, F., Sanin, D.E., Edwards-Hicks, J., Villa, M., Kabat, A.M., Kamiński, M.M., Stanckzak, M., Weiss, H.J., Grzes, K.M., et al. (2021). Polyamine metabolism is a central determinant of helper T cell lineage fidelity. Cell *184*, 4186–4202.e20. https://doi.org/10.1016/j.cell.2021.06.007.
29. Bowlin, T.L., McKown, B.J., Babcock, G.F., and Sunkara, P.S. (1987). Intracellular polyamine biosynthesis is required for interleukin 2 responsiveness during lymphocyte mitogenesis. Cell. Immunol. *106*, 420–427. https://doi.org/10.1016/0008-8749(87)90184-5.
30. Kay, J.E., and Pegg, A.E. (1973). Effect of inhibition of spermidine formation on protein and nucleic acid synthesis during lymphocyte activation. FEBS Lett. *29*, 301–304. https://doi.org/10.1016/0014-5793(73)80044-4.
31. Scott, I.G., Pösö, H., Akerman, K.E., and Andersson, L.C. (1985). Rapid activation of ornithine decarboxylase by mitogenic (but not by nonmitogenic) ligands in human T lymphocytes. Eur. J. Immunol. *15*, 783–787. https://doi.org/10.1002/eji.1830150808.
32. Schall, R.P., Sekar, J., Tandon, P.M., and Susskind, B.M. (1991). Difluoromethylornithine (DFMO) arrests murine CTL development in the late, pre-effector stage. Immunopharmacology *21*, 129–143. https://doi.org/10.1016/0162-3109(91)90016-r.
33. Wang, R., Dillon, C.P., Shi, L.Z., Milasta, S., Carter, R., Finkelstein, D., McCormick, L.L., Fitzgerald, P., Chi, H., Munger, J., and Green, D.R. (2011). The transcription factor Myc controls metabolic reprogramming upon T lymphocyte activation. Immunity *35*, 871–882. https://doi.org/10.1016/j.immuni.2011.09.021.
34. Klysz, D., Tai, X., Robert, P.A., Craveiro, M., Cretenet, G., Oburoglu, L., Mongellaz, C., Floess, S., Fritz, V., Matias, M.I., et al. (2015). Glutamine-dependent alpha-ketoglutarate production regulates the balance between T helper 1 cell and regulatory T cell generation. Sci. Signal. *8*, ra97. https://doi.org/10.1126/scisignal.aab2610.
35. Johnson, M.O., Wolf, M.M., Madden, M.Z., Andrejeva, G., Sugiura, A., Contreras, D.C., Maseda, D., Liberti, M.V., Paz, K., Kishton, R.J., et al. (2018). Distinct regulation of Th17 and Th1 cell differentiation by glutaminase-dependent metabolism. Cell *175*, 1780–1795.e19. https://doi.org/10.1016/j.cell.2018.10.001.
36. Yoo, H.C., Yu, Y.C., Sung, Y., and Han, J.M. (2020). Glutamine reliance in cell metabolism. Exp. Mol. Med. *52*, 1496–1516. https://doi.org/10.1038/s12276-020-00504-8.
37. Wicker, C.A., Hunt, B.G., Krishnan, S., Aziz, K., Parajuli, S., Palackdharry, S., Elaban, W.R., Wise-Draper, T.M., Mills, G.B., Waltz, S.E., and Takiar, V. (2021). Glutaminase inhibition with telaglenastat (CB-839) improves treatment response in combination with ionizing radiation in head and neck squamous cell carcinoma models. Cancer Lett. *502*, 180–188. https://doi.org/10.1016/j.canlet.2020.12.038.

38. Song, M., Kim, S.H., Im, C.Y., and Hwang, H.J. (2018). Recent development of small molecule glutaminase inhibitors. Curr. Top. Med. Chem. *18*, 432–443. https://doi.org/10.2174/1568026618666180525100830.

39. Garber, K. (2016). Cancer anabolic metabolism inhibitors move into clinic. Nat. Biotechnol. *34*, 794–795. https://doi.org/10.1038/nbt0816-794.

40. Kim, M., Gwak, J., Hwang, S., Yang, S., and Jeong, S.M. (2019). Mitochondrial GPT2 plays a pivotal role in metabolic adaptation to the perturbation of mitochondrial glutamine metabolism. Oncogene *38*, 4729–4738. https://doi.org/10.1038/s41388-019-0751-4.

41. Kolev, M., Dimeloe, S., Le Friec, G., Navarini, A., Arbore, G., Povoleri, G.A., Fischer, M., Belle, R., Loeliger, J., Develioglu, L., et al. (2015). Complement regulates nutrient influx and metabolic reprogramming during Th1 cell responses. Immunity *42*, 1033–1047. https://doi.org/10.1016/j.immuni.2015.05.024.

42. Arbore, G., Ong, V.H., Costantini, B., Denton, C.P., Abraham, D., Placais, L., Blighe, K., Mitchell, L., Ellis, R., Heck, S., et al. (2020). Deep phenotyping detects a pathological CD4(+) T cell complosome signature in systemic sclerosis. Cell. Mol. Immunol. *17*, 1010–1013. https://doi.org/10.1038/s41423-019-0360-8.

43. Le Friec, G., Sheppard, D., Whiteman, P., Karsten, C.M., Shamoun, S.A., Laing, A., Bugeon, L., Dallman, M.J., Melchionna, T., Chillakuri, C., et al. (2012). The CD46-Jagged1 interaction is critical for human TH1 immunity. Nat. Immunol. *13*, 1213–1221. https://doi.org/10.1038/ni.2454.

44. Werner, A., Amann, E., Schnitzius, V., Habermeier, A., Luckner-Minden, C., Leuchtner, N., Rupp, J., Closs, E.I., and Munder, M. (2016). Induced arginine transport via cationic amino acid transporter-1 is necessary for human T cell proliferation. Eur. J. Immunol. *46*, 92–103. https://doi.org/10.1002/eji.201546047.

45. Sin, Y.Y., Baron, G., Schulze, A., and Funk, C.D. (2015). Arginase-1 deficiency. J. Mol. Med. (Berl.) *93*, 1287–1296. https://doi.org/10.1007/s00109-015-1354-3.

46. Caldwell, R.W., Rodriguez, P.C., Toque, H.A., Narayanan, S.P., and Caldwell, R.B. (2018). Arginase: A multifaceted enzyme important in health and disease. Physiol. Rev. *98*, 641–665. https://doi.org/10.1152/physrev.00037.2016.

47. Das, P., Lahiri, A., Lahiri, A., and Chakravortty, D. (2010). Modulation of the arginase pathway in the context of microbial pathogenesis: a metabolic enzyme moonlighting as an immune modulator. PLoS Pathog. *6*, e1000899. https://doi.org/10.1371/journal.ppat.1000899.

48. Tommasi, S., Elliot, D.J., Da Boit, M., Gray, S.R., Lewis, B.C., and Mangoni, A.A. (2018). Homoarginine and inhibition of human arginase activity: kinetic characterization and biological relevance. Sci. Rep. *8*, 3697. https://doi.org/10.1038/s41598-018-22099-x.

49. Matias, M.I., Yong, C.S., Foroushani, A., Goldsmith, C., Mongellaz, C., Sezgin, E., Levental, K.R., Talebi, A., Perrault, J., Rivière, A., et al. (2021). Regulatory T cell differentiation is controlled by alphaKG-induced alterations in mitochondrial metabolism and lipid homeostasis. Cell Rep. *37*, 109911. https://doi.org/10.1016/j.celrep.2021.109911.

50. Yang, W.H., Qiu, Y., Stamatatos, O., Janowitz, T., and Lukey, M.J. (2021). Enhancing the efficacy of glutamine metabolism inhibitors in cancer therapy. Trends Cancer *7*, 790–804. https://doi.org/10.1016/j.trecan.2021.04.003.

51. Halama, A., and Suhre, K. (2022). Advancing cancer treatment by targeting glutamine metabolism-A roadmap. Cancers (Basel) *14*, 553. https://doi.org/10.3390/cancers14030553.

52. Chang, C.H., Curtis, J.D., Maggi, L.B., Jr., Faubert, B., Villarino, A.V., O'Sullivan, D., Huang, S.C., van der Windt, G.J., Blagih, J., Qiu, J., et al. (2013). Posttranscriptional control of T cell effector function by aerobic glycolysis. Cell *153*, 1239–1251. https://doi.org/10.1016/j.cell.2013.05.016.

53. Mitra, D., Vega-Rubin-de-Celis, S., Royla, N., Bernhardt, S., Wilhelm, H., Tarade, N., Poschet, G., Buettner, M., Binenbaum, I., Borgoni, S., et al. (2021). Abrogating GPT2 in triple-negative breast cancer inhibits tumor growth and promotes autophagy. Int. J. Cancer *148*, 1993–2009. https://doi.org/10.1002/ijc.33456.

54. Roers, A., Siewe, L., Strittmatter, E., Deckert, M., Schlüter, D., Stenzel, W., Gruber, A.D., Krieg, T., Rajewsky, K., and Müller, W. (2004). T cell-specific inactivation of the interleukin 10 gene in mice results in enhanced T cell responses but normal innate responses to lipopolysaccharide or skin irritation. J. Exp. Med. *200*, 1289–1297. https://doi.org/10.1084/jem.20041789.

55. Belkaid, Y., Hoffmann, K.F., Mendez, S., Kamhawi, S., Udey, M.C., Wynn, T.A., and Sacks, D.L. (2001). The role of interleukin (IL)-10 in the persistence of Leishmania major in the skin after healing and the therapeutic potential of anti-IL-10 receptor antibody for sterile cure. J. Exp. Med. *194*, 1497–1506. https://doi.org/10.1084/jem.194.10.1497.

56. Dai, W.J., Köhler, G., and Brombacher, F. (1997). Both innate and acquired immunity to Listeria monocytogenes infection are increased in IL-10-deficient mice. J. Immunol. *158*, 2259–2267.

57. Brooks, D.G., Trifilo, M.J., Edelmann, K.H., Teyton, L., McGavern, D.B., and Oldstone, M.B. (2006). Interleukin-10 determines viral clearance or persistence in vivo. Nat. Med. *12*, 1301–1309. https://doi.org/10.1038/nm1492.

58. Neumann, C., Scheffold, A., and Rutz, S. (2019). Functions and regulation of T cell-derived interleukin-10. Semin. Immunol. *44*, 101344. https://doi.org/10.1016/j.smim.2019.101344.

59. Roncarolo, M.G., Gregori, S., Bacchetta, R., Battaglia, M., and Gagliani, N. (2018). The biology of T regulatory type 1 cells and their therapeutic application in immune-mediated diseases. Immunity *49*, 1004–1019. https://doi.org/10.1016/j.immuni.2018.12.001.

60. Clemente, G.S., van Waarde, A., Antunes, I.F., Dömling, A., and Elsinga, P.H. (2020). Arginase as a potential biomarker of disease progression: a molecular imaging perspective. Int. J. Mol. Sci. *21*, 5291. https://doi.org/10.3390/ijms21155291.

61. Grzywa, T.M., Sosnowska, A., Matryba, P., Rydzynska, Z., Jasinski, M., Nowis, D., and Golab, J. (2020). Myeloid cell-derived arginase in cancer immune response. Front. Immunol. *11*, 938. https://doi.org/10.3389/fimmu.2020.00938.

62. Mills, C.D. (2012). M1 and M2 macrophages: oracles of health and disease. Crit. Rev. Immunol. *32*, 463–488. https://doi.org/10.1615/critrevimmunol.v32.i6.10.

63. Yang, Z., and Ming, X.F. (2014). Functions of arginase isoforms in macrophage inflammatory responses: impact on cardiovascular diseases and metabolic disorders. Front. Immunol. *5*, 533. https://doi.org/10.3389/fimmu.2014.00533.

64. Wang, G., Liszewski, M.K., Chan, A.C., and Atkinson, J.P. (2000). Membrane cofactor protein (MCP; CD46): isoform-specific tyrosine phosphorylation. J. Immunol. *164*, 1839–1846. https://doi.org/10.4049/jimmunol.164.4.1839.

65. Mueller, S.N., Langley, W.A., Li, G., García-Sastre, A., Webby, R.J., and Ahmed, R. (2010). Qualitatively different memory CD8+ T cells are generated after lymphocytic choriomeningitis virus and influenza virus infections. J. Immunol. *185*, 2182–2190. https://doi.org/10.4049/jimmunol.1001142.

66. Lavanya, M., Kinet, S., Montel-Hagen, A., Mongellaz, C., Battini, J.L., Sitbon, M., and Taylor, N. (2008). Cell surface expression of the bovine leukemia virus-binding receptor on B and T lymphocytes is induced by receptor engagement. J. Immunol. *181*, 891–898. https://doi.org/10.4049/jimmunol.181.2.891.

67. Langmead, B., and Salzberg, S.L. (2012). Fast gapped-read alignment with Bowtie 2. Nat. Methods *9*, 357–359. https://doi.org/10.1038/nmeth.1923.

68. Liao, Y., Smyth, G.K., and Shi, W. (2019). The R package Rsubread is easier, faster, cheaper and better for alignment and quantification of RNA sequencing reads. Nucleic Acids Res. *47*, e47. https://doi.org/10.1093/nar/gkz114.

69. Robinson, M.D., McCarthy, D.J., and Smyth, G.K. (2010). edgeR: a Bioconductor package for differential expression analysis of digital gene expression data. Bioinformatics *26*, 139–140. https://doi.org/10.1093/bioinformatics/btp616.

70. Subramanian, A., Tamayo, P., Mootha, V.K., Mukherjee, S., Ebert, B.L., Gillette, M.A., Paulovich, A., Pomeroy, S.L., Golub, T.R., Lander, E.S., and Mesirov, J.P. (2005). Gene set enrichment analysis: a knowledge-based approach for interpreting genome-wide expression profiles. Proc. Natl. Acad. Sci. USA *102*, 15545–15550. https://doi.org/10.1073/pnas.0506580102.

71. Ritchie, M.E., Phipson, B., Wu, D., Hu, Y., Law, C.W., Shi, W., and Smyth, G.K. (2015). limma powers differential expression analyses for RNA-sequencing and microarray studies. Nucleic Acids Res. *43*, e47. https://doi.org/10.1093/nar/gkv007.

72. Liberzon, A., Birger, C., Thorvaldsdóttir, H., Ghandi, M., Mesirov, J.P., and Tamayo, P. (2015). The Molecular Signatures Database (MSigDB) hallmark gene set collection. Cell Syst. *1*, 417–425. https://doi.org/10.1016/j.cels.2015.12.004.

73. El Kasmi, K.C., Qualls, J.E., Pesce, J.T., Smith, A.M., Thompson, R.W., Henao-Tamayo, M., Basaraba, R.J., König, T., Schleicher, U., Koo, M.S., et al. (2008). Toll-like receptor-induced arginase 1 in macrophages thwarts effective immunity against intracellular pathogens. Nat. Immunol. *9*, 1399–1406. https://doi.org/10.1038/ni.1671.

74. Shi, O., Morris, S.M., Jr., Zoghbi, H., Porter, C.W., and O'Brien, W.E. (2001). Generation of a mouse model for arginase II deficiency by targeted disruption of the arginase II gene. Mol. Cell. Biol. *21*, 811–813. https://doi.org/10.1128/MCB.21.3.811-813.2001.

75. Schluns, K.S., Williams, K., Ma, A., Zheng, X.X., and Lefrançois, L. (2002). Cutting edge: requirement for IL-15 in the generation of primary and memory antigen-specific CD8 T cells. J. Immunol. *168*, 4827–4831. https://doi.org/10.4049/jimmunol.168.10.4827.

76. Yang, G., Hisha, H., Cui, Y., Fan, T., Jin, T., Li, Q., Lian, Z., Hosaka, N., Li, Y., and Ikehara, S. (2002). A new assay method for late CFU-S formation and long-term reconstituting activity using a small number of pluripotent hemopoietic stem cells. Stem Cells *20*, 241–248. https://doi.org/10.1634/stemcells.20-3-241.

77. Janowska-Wieczorek, A., Majka, M., Kijowski, J., Baj-Krzyworzeka, M., Reca, R., Turner, A.R., Ratajczak, J., Emerson, S.G., Kowalska, M.A., and Ratajczak, M.Z. (2001). Platelet-derived microparticles bind to hematopoietic stem/progenitor cells and enhance their engraftment. Blood *98*, 3143–3149. https://doi.org/10.1182/blood.v98.10.3143.

78. Muench, L.J.R.a.H. (1938). A simple method of estimating fifty percent endpoints. Am. J. Hyg. *27*, 493–497.

79. Sumner, L.W., Amberg, A., Barrett, D., Beale, M.H., Beger, R., Daykin, C.A., Fan, T.W., Fiehn, O., Goodacre, R., Griffin, J.L., et al. (2007). Proposed minimum reporting standards for chemical analysis Chemical Analysis Working Group (CAWG) Metabolomics Standards Initiative (MSI). Metabolomics *3*, 211–221. https://doi.org/10.1007/s11306-007-0082-2.

80. Milne, S.B., Mathews, T.P., Myers, D.S., Ivanova, P.T., and Brown, H.A. (2013). Sum of the parts: mass spectrometry-based metabolomics. Biochemistry *52*, 3829–3840. https://doi.org/10.1021/bi400060e.

81. Sharma, G., Attri, S.V., Behra, B., Bhisikar, S., Kumar, P., Tageja, M., Sharda, S., Singhi, P., and Singhi, S. (2014). Analysis of 26 amino acids in human plasma by HPLC using AQC as derivatizing agent and its application in metabolic laboratory. Amino Acids *46*, 1253–1263. https://doi.org/10.1007/s00726-014-1682-6.

82. Zhang, J., Ahn, W.S., Gameiro, P.A., Keibler, M.A., Zhang, Z., and Stephanopoulos, G. (2014). 13C isotope-assisted methods for quantifying glutamine metabolism in cancer cells. Methods Enzymol. *542*, 369–389. https://doi.org/10.1016/B978-0-12-416618-9.00019-4.

83. Wickham, H. (2016). ggplot2: Elegant Graphics for Data Analysis (Springer).

Please cite this article in press as: West et al., Loss of CD4+ T cell-intrinsic arginase 1 accelerates Th1 response kinetics and reduces lung pathology during influenza infection, Immunity (2023), https://doi.org/10.1016/j.immuni.2023.07.014

STAR★METHODS

KEY RESOURCES TABLE

REAGENT or RESOURCE	SOURCE	IDENTIFIER
Antibodies		
APC anti-mouse CD3 (17A2)	Biolegend	Cat# 100236; RRID: AB_2561456
Brilliant Violet 510™ anti-mouse CD3 (17A2)	Biolegend	Cat# 100233; RRID: AB_2561387
FITC anti-mouse CD4 (RMA4-5)	Biolegend	Cat# 100510; RRID: AB_312713
Alexa Fluor® 488 anti-mouse CD4 (RMA4-5)	Biolegend	Cat# 100530; RRID: AB_389325
Brilliant Violet 421™ anti-mouse CD4 (RMA4-5)	Biolegend	Cat# 100544; RRID: AB_11219790
Brilliant Violet 605™ anti-mouse CD4 (RMA4-5	Biolegend	Cat #100548; RRID: AB_2563054
PerCP/Cyanine5.5 anti-mouse CD8a (53-6.7)	Biolegend	Cat# 100734; RRID: AB_2075238
Brilliant Violet 711™ anti-mouse CD8a (53-6.7)	Biolegend	Cat# 100748; RRID: AB_2562100
PE anti-mouse CD11a (I21/7)	Biolegend	Cat# 153104; RRID: AB_2716034
PerCP/Cyanine5.5 anti-mouse CD11a (I21/7)	Biolegend	Cat# 101124; RRID: AB_2562932
Brilliant Violet 605™ anti-mouse CD11b (M1/70)	Biolegend	Cat # 101257; RRID: AB_2565431
PE anti-mouse CD25 (PC61)	Biolegend	Cat# 102008; RRID: AB_312857
APC anti-mouse CD25 (PC61)	Biolegend	Cat# 102012; RRID: AB_312861
FITC anti-mouse CD45RB (C363-16A)	Biolegend	Cat# 103306; RRID: AB_313013
PE-Cyanine7 anti-mouse CD49d (R1-2)	Biolegend	Cat# 103618; RRID: AB_2563700
APC anti-mouse CD62L (MEL-14)	Biolegend	Cat# 104412; RRID: AB_313099
Alexa Fluor® 488 anti-mouse CD44 (IM7)	Biolegend	Cat# 103016; RRID: AB_493679
PerCP anti-mouse CD44 (IM7)	Biolegend	Cat# 103036; RRID: AB_10645506
Brilliant Violet 421™ anti-mouse CD44 (IM7)	Biolegend	Cat# 103040; RRID: AB_2616903
PerCp/Cyanine5.5 anti-mouse CD45.1 (A20)	Biolegend	Cat# 110728; RRID: AB_893346
APC-Cyanine7 anti-mouse CD45.1 (A20)	Biolegend	Cat# 110716; RRID: AB_313505
Brilliant Violet 421™ anti-mouse CD45.1 (A20)	Biolegend	Cat# 110732; RRID: AB_2562563
Percp anti-mouse CD45.2 (104)	Biolegend	Cat# 109828; RRID: AB_893350
Alexa Fluor® 488 anti-mouse CD45.2 (104)	Biolegend	Cat# 109816; RRID: AB_492868
Brilliant Violet 510™ anti-mouse CD90.2 (53-2.1)	Biolegend	Cat# 140319; RRID: AB_2561395
Alexa Fluor® 488 anti-mouse CD107a (1D4B)	Biolegend	Cat# 121608; RRID: AB_571983
Alexa Fluor® 488 anti-mouse CD107b (M3/84)	Biolegend	Cat# 108510; RRID: AB_493308
Alexa Fluor® 647 anti-mouse FoxP3 (150D)	Biolegend	Cat# 320014; RRID: AB_439750
Alexa Fluor® 647 anti-mouse GR1 (RB6-8C5)	Biolegend	Cat# 108418; RRID: AB_389331
Brilliant Violet 421™ anti-mouse IL-2 (JES6-5H4)	Biolegend	Cat# 503826; RRID: AB_2650897
Brilliant Violet 421™ anti-mouse IL-4 (11B11)	Biolegend	Cat# 504120; RRID: AB_2562102

(*Continued on next page*)

Please cite this article in press as: West et al., Loss of CD4+ T cell-intrinsic arginase 1 accelerates Th1 response kinetics and reduces lung pathology during influenza infection, Immunity (2023), https://doi.org/10.1016/j.immuni.2023.07.014

Continued

REAGENT or RESOURCE	SOURCE	IDENTIFIER
Alexa Fluor® 647 anti-mouse IL-10 (JESS-16E3)	Biolegend	Cat# 505014; RRID: AB_493511
PE anti-mouse IL-17A (TC11-1810.1)	Biolegend	Cat# 506904; RRID: AB_315464
Brilliant Violet 711™ anti-mouse IL-17A (TC11-1810.1)	Biolegend	Cat# 506941; RRID: AB_2565836
Alexa Fluor® 488 anti-mouse IFNg (XMG1.2)	Biolegend	Cat# 505813; RRID: AB_493312
Brilliant Violet 421™ anti-mouse IFNg (XMG1.2)	Biolegend	Cat# 505830; RRID: AB_2563105
PE anti-mouse/human Ki67 (B56)	BD Biosciences	Cat # 567719; RRID: AB_2916708
Brilliant Violet 711™ anti-mouse/human Ki67 (B56)	BD Biosciences	Cat# 563755; RRID: AB_2738406
Alexa Fluor® 647 anti-Phospho-S6 ribosomal protein (D68F8)	Cell Signaling Technology	Cat #5044; RRID: AB_10829359
Brilliant Violet 510™ anti-mouse TCRb (H57-597)	Biolegend	Cat# 109234; RRID: AB_2562350
APC anti-Tbet/Tbx21 (4B10)	Biolegend	Cat# 644814; RRID: AB_10901173
PE-Cyanine7 anti-mouse TNFa (MP6-XT22)	Biolegend	Cat# 506324; RRID: AB_2256076
PE anti-mouse/human Arginase 1 (A1exF5)	eBiosciences/Invitrogen	Cat# 12-3697-82; RRID: AB_2734839
Alexa Fluor® 488 anti- pSTAT1 pY701	BD Biosciences	Cat # 612596; RRID: AB_399879
PE anti-STAT4 pY693	BD Biosciences	Cat# 558249; RRID: AB_397066
anti-mouse GPT2	Proteintech/Invitrogen	Cat# 16757-1-AP; RRID: AB_2112098
PE anti-human ARG1 (14D2C43)	Biolegend	Cat# 369704; RRID: AB_2571900
Alexa Fluor® 647 anti-human CD197/CCR7 (G043H7)	Biolegend	Cat# 353218: RRID: AB_10917385
FITC anti-human CD4 (RPA-T4)	Biolegend	Cat# 300506: RRID: AB_314074
PE anti-human CD8 (SK1)	Biolegend	Cat# 344706: RRID: AB_1953244
PE-Cyanine7 anti-human CD45RO (UCHL1)	Biolegend	Cat# 304230: RRID: AB_11203900
Pacific Blue anti-human CD45RA (HI100)	Biolegend	Cat# 304118; RRID: AB_493657
Alexa Fluor® 647 anti-human IFNg (4S.B3)	Biolegend	Cat# 502516; RRID:AB_493031
Brilliant Violet 421™ anti-human IL-10 (JES3-9D7)	Biolegend	Cat# 501422: RRID: AB_2632952
Brilliant Violet 711™ anti-human IL-17A (BL168)	Biolegend	Cat# 512328; RRID: AB_2563888
PE-Cyanine7 anti-human IL-4 (MP4-25D2)	Biolegend	Cat# 500824; RRID: AB_2126746
PE anti-human TNFa (MAb11)	Biolegend	Cat# 502909; RRID: AB_315261
anti-mouse CD3 (145-2C11)	BioXcell	Cat# BE0001-1; RRID: AB_1107634
anti-mouse CD28 (37.51)	BioXcell	Cat # BE0015-1; RRID: AB_1107624
anti-human CD3 (OKT3)	BioXcell	Cat# BE0001-2; RRID: AB_1107632
anti-human CD28 (CD28.2)	BD Biosciences	Cat # 555725; RRID: AB_396068
anti-human CD46 (TRA2-10)	Washington University Hybridoma Center (WUHC)	Clone TRA-2-10; Wang et al.[64]
anti-mouse IL-4 (1B11)	BioXcell	Cat # BE0045; RRID: AB_1107707
Alexa Fluor® 488 goat anti-rabbit IgG1 secondary Ab	Invitrogen	Cat# A11034; RRID: AB_2576217
Bacterial and virus strains		
Influenza PR8-33 (H1N1)	Mueller et al.[65]	N/A
Biological samples		
Healthy donor blood buffy coats	NIH blood Bank (NIH)	N/A

(*Continued on next page*)

Please cite this article in press as: West et al., Loss of CD4+ T cell-intrinsic arginase 1 accelerates Th1 response kinetics and reduces lung pathology during influenza infection, Immunity (2023), https://doi.org/10.1016/j.immuni.2023.07.014

Continued

REAGENT or RESOURCE	SOURCE	IDENTIFIER
Healthy donor freshly drawn blood	NIH blood Bank or University Children's Hospital Zurich Switzerland or Medical University of Innsbruck Austria	N/A
Blood samples from pediatric ARG1 deficient patients	University Children's Hospital Zurich Switzerland or Medical University of Innsbruck Austria	N/A
T cells isolated from WT, Arg1 KO or Arg2 KO mice	NIH	N/A
Chemicals, peptides, and recombinant proteins		
Brilliant Violet conjugated NP311-325 tetramer	NIH tetramer core facility	N/A
Rabbit Fc-tagged BLV-RBD (BLV.RBD.rabbitIgG1-Fc)	Metafora-biosystems	Lavanya et al.[66]
Recombinant mouse IL-12 protein	Biolegend	Cat # 577004
Recombinant mouse IL-7 protein	Biolegend	Cat # 577804
Recombinant human IL-2 protein	Peprotech	Cat # 200-02
Recombinant mouse GM-CSF	Biolegend	Cat # 576304
LIVE/DEAD™ Fixable Near-IR	Invitrogen	Cat # L10119
LIVE/DEAD™ Fixable Aqua	Invitrogen	Cat # L34965
Cell trace violet	Invitrogen	Cat # C34557
NorNOHA	Cayman Chemicals	Cat # 10006861
Aminooxyacetate	Cayman Chemicals	Cat # 28298
di-methyl 2-ooxoglutarate	Sigma-Aldrich	Cat # 349631
Recombinant ARG1 his-tag protein	BPS Biosciences	Cat # 71658
Phorbol 12-myristate 13-acetate (PMA)	Sigma-Aldrich	Cat # P1585
Protein Transport inhibitor	Thermo-Fisher	Cat # 00-4980-03
Ionomycin	Sigma-Aldrich	Cat # 13909
oligomycin	Sigma-Aldrich	Cat # O4876
Carbonyl cyanide-4-(trifluoromethoxy) phenylhydrazone (FCCP)	Sigma-Aldrich	Cat # C2920
rotenone	Sigma-Aldrich	Cat # R8875
Antimycin A	Sigma-Aldrich	Cat # A8674
2-NBDG	Cayman Chemicals	Cat # 11046
TPCK-trypsin	ThermoFisher	Cat # 20233
Critical commercial assays		
Phosphoflow fix buffer I	BD biosciences	Cat # 557870
Phosphoflow perm buffer III	BD biosciences	Cat # 554656
BD cytofix/cytoperm kit	BD biosciences	Cat # 554714
Ebioscience™ Foxp3/Transcription Factor Staining Buffer Set	Invitrogen	Cat # 00-5523-00
Mouse CD3e depletion kit	Miltenyi Biotech	Cat # (# 130-094-973
Mouse CD4 T cell isolation kit	Miltenyi Biotech	Cat # #130-104-454
Mouse CD4 T cell isolation kit	Stem Cell Technologies	Cat # 19852
Human CD4 T cell isolation kit	Miltenyi Biotech	Cat # 130-091-155
Human CD4 T cell isolation kit	Stem Cell Technologies	Cat # 17952
Click-iT™ EDU Alexa Fluor™ 647 Flow cytometry Assay Kit	Thermofisher	Cat # C10424
Click-iT™ EDU Alexa Fluor™ 488 Flow cytometry Assay Kit	Thermofisher	Cat # C10425
P3 primary Cell 4D-Nucleofector X kit S	Lonza	Cat # V4XP-3032

(*Continued on next page*)

Please cite this article in press as: West et al., Loss of CD4+ T cell-intrinsic arginase 1 accelerates Th1 response kinetics and reduces lung pathology during influenza infection, Immunity (2023), https://doi.org/10.1016/j.immuni.2023.07.014

Continued

REAGENT or RESOURCE	SOURCE	IDENTIFIER
p180 targeted quantification kit	Biocrates	N/A
LEGENDplex™ Human T helper cytokine panel	Biolegend	Cat # 741028
LEGENDplex™ Human Inflammation panel	Biolegend	Cat # 740809
LEGENDplex™ Mouse T helper cytokine panel	Biolegend	Cat # 741044
LEGENDplex™ Mouse Inflammation panel	Biolegend	Cat # 740446
Mouse IL-10 enhanced sensitivity flex set	BD biosciences	Cat # 562263; RRD: AB_2869410
RNAqueous Micro Kit	Invitrogen	Cat # AM1931
NEBNext® Ultra™ II RNA Library Prep Kit for Illumina®	NEB	Cat # E7770
NEBNext® Poly(A) mRNA Magnetic Isolation Module	NEB	Cat # E7490
Deposited data		
RNA seq of lung/spleen CD4 T cells after influenza	This paper	GEO: GSE214241
RNA seq of in vitro activated CD4 T cells	This paper	GEO: GSE214241
Microarray of human CD4 T cells	This paper	GEO: GSE229775
Unbiased metabolomics data	This paper	MassIVE; MSV000090368
RNA seq	Johnson et al.[35]	GEO: GSE112244
Experimental models: Cell lines		
MDCK cells (NBL-2)	ATCC	Cat# CCL-34; RRID:CVCL_0422
Experimental models: Organisms/strains		
Mouse: *Arg1*^{flox}	Jackson laboratory	IMSR_JAX:008817
Mouse: CD4cre	Jackson laboratory	IMSR_JAX:022071
Mouse: *Arg2* KO	Jackson laboratory	IMSR_JAX:020286
Mouse: Rag1 KO	Jackson laboratory	IMSR_JAX:002216
Mouse: B6 CD45.1	Jackson laboratory	IMSR_JAX:002014
Mouse: C57BL/10 Rag2$^{-/-}$	Taconic	Line # 103
Oligonucleotides		
Alt-R CRISPR-Cas9 tracrRNA	Integrated DNA Technologies	Cat # 1072534
Non-targeting control gRNA	Addgene	Cat # BRDN0001149198
Cas9 nuclease	Integrated DNA Technologies	Cat # 1081059
Software and algorithms		
Adobe® Illustrator 2021	Adobe	https://www.adobe.com/adobe/illustrator
FlowJo 10 software	Treestar	https://www.flowjo.com/
Bowtie2	Langmead and Salzberg[67]	https://bowtie-bio.sourceforge.net/bowtie2/index.shtml
RSubread/v 2.8.1	Liao et al.[68]	https://bioconductor.org
EdgeR/v 3.36.0	Robinson et al.[69]	https://bioconductor.org
GraphPad PRISM 9.4.1	Graphpad software	https://www.graphpad.com
GSEA version 3.0	Subramanian et al.[70]	https://www.gsea-msgdb.org
Limma	Ritchie et al.[71]	https://bioconductor.org
Molecular Signatures Database v.7.5.1	Liberzon et al.[72]	https://www.gsea-msigdb.org/gsea/msigdb/annotate.jsp
Morpheus	Broad institute	https://software.broadinstitute.org/morpheus
DataGraph v 5.0	Visual Data Tools, Inc	https://visualdatatools.com
Other		
PBS	Corning	Cat # 21-040-CV

(*Continued on next page*)

Please cite this article in press as: West et al., Loss of CD4+ T cell-intrinsic arginase 1 accelerates Th1 response kinetics and reduces lung pathology during influenza infection, Immunity (2023), https://doi.org/10.1016/j.immuni.2023.07.014

Continued

REAGENT or RESOURCE	SOURCE	IDENTIFIER
RPMI	ThermoFisher	Cat # 21870-076
IMDM	ThermoFisher	Cat # 12440-053
HBSS	ThermoFisher	Cat # 14170-112
Collagenase	Sigma-Aldrich	Cat # C7657
DNAse I	Sigma-Aldrich	Cat # DN25
Percoll® Cytvia	Sigma-Aldrich	Cat # GE17-0891-01
FBS	Sigma-Aldrich	Cat # F0926
Seahorse XF RPMI medium	Agilent Technologies	Cat # 103576-100
Cell-Tak	Corning	Cat # 354241
HEPES	Corning	Cat # 25-060-CI
DMEM	ThermoFisher	Cat # 11320-033
PenicIllin-Streptomycin	ThermoFisher	Cat # 15070-63
13C-Glutamine	Cambridge Isotope Laboratories, Inc.	Cat # CLM-1822-H-0.25
Glutamine	ThermoFisher	Cat # 25030-081

RESOURCE AVAILABILITY

Lead contact

Further information and requests for resources and reagents should be directed to and will be fulfilled by the lead contact Claudia Kemper (claudia.kemper@nih.gov).

Materials availability

This study did not generate new unique reagents.

Data and code availability

- RNA seq data and microarray data have been deposited at GEO and the unbiased metabolomics data is deposited in MassIVE. All data are publicly available as of the date of publication. Accession numbers are listed in the key resources table.
- This paper analyzes existing, publicly available data. The accession number for this dataset is listed in the key resources table.
- This paper does not report original code.
- All data reported in this paper will be shared by the lead contact upon request. Any additional information required to reanalyze the data reported in this paper is available from the lead contact upon request.

Gene expression values obtained through RNA-sequencing of CD4+ T cells isolated from the lungs and spleens of wild type (WT) mice infected with influenza virus at day 9 post infection are deposited in the NCBI Gene Expression Omnibus (GEO) under accession code GSE214241. Gene expression values obtained through RNA-sequencing of splenic CD4+ T cells from CD4cre− *Arg1*$^{fl/fl}$ (WT), CD4cre+ *Arg1*$^{fl/fl}$ (*Arg1* KO), and global arginase 2-deficient (*Arg2* KO) mice 22 hours post anti-CD3 and anti-CD28 *in vitro* activation are deposited in the NCBI Gene Expression Omnibus (GEO) under accession code GEO: GSE214241. Gene expression values obtained through microarray of CD4+ T cells from healthy donor and patients with arginase 1-deficiency 6 hours post anti-CD3 and anti-CD46 *in vitro* activation are deposited in NCBI GEO under accession code GEO: GSE229775. The unbiased metabolomics data is deposited in Mass Spectometry Interactive Virtual Environment (MassIVE) under accession code MassIVE: MSV000090368.

EXPERIMENTAL MODEL AND STUDY PARTICIPANT DETAILS

Healthy human donors and patients

Blood samples were obtained and processed with appropriate ethical and institutional approvals. All healthy donors and the patients' parents gave informed consent prior to sample collection. CD4+ T cells from adult healthy volunteers were purified from freshly drawn blood or from buffy coats (both NIH Blood Bank, Bethesda, USA) and activated as described in method details. Detailed information on the four patients with arginase 1 -deficiency is provided in Table S4.

Mice

Arg1^{flox} mice (strain # 008817), CD4cre mice (strain # 022071), *Arg2* KO mice (strain # 020286), Rag1 KO (strain # 002216) and B6 CD45.1 mice (strain # 002014) are all on the C57BL/6J background and were obtained from Jackson Laboratories.[18,73–77] The *Arg1*^{flox} mice were bred to the CD4cre mice to generate *Arg1*$^{fl/fl}$ CD4cre+ mice. The C57BL/10 Rag2$^{-/-}$ mice were obtained from

Please cite this article in press as: West et al., Loss of CD4+ T cell-intrinsic arginase 1 accelerates Th1 response kinetics and reduces lung pathology during influenza infection, Immunity (2023), https://doi.org/10.1016/j.immuni.2023.07.014

Taconic. The appropriate littermate mice were used as WT controls (WT, *Arg1*$^{fl/fl}$ CD4cre^{-} or WT CD4cre^{+}). Both female and male mice were used to equal parts and all mice were housed at ~22 °C. All mice were maintained in BSL2 AALAC-accredited facilities at the NIH and were performed in compliance with an animal study proposal approved by the NHLBI Animal Care and Use Committee.

METHOD DETAILS

Antibodies, proteins and inhibitors

Inhibitors and metabolites

The pan arginase inhibitor NorNOHA (150uM; #10006861, Cayman Chemicals) or the GPT2 inhibitor Aminooxyacetate (AOA; 100uM, #28298, Cayman Chemicals) or the cell soluble form of 2-oxoglutarate (αKG) (di-methyl 2-ooxoglutarate; 1.5mM, #349631, Sigma-Aldrich) were added into the *in vitro* cell cultures at the time of stimulation. Recombinant ARG1 his-tag protein was from BPS Biosciences (#71658).

Mouse Flow cytometry antibodies/reagents

The following antibodies were used to perform flow cytometry on mouse cells (all antibodies are from Biolegend unless indicated otherwise): anti-CD3 (clone 17A2), CD4 (clone RMA-4), CD8 (clone 53-6.7), CD11a (clone I21/7), CD11b (clone M1/70), CD25 (clone PC-61), CD45RB (clone C363-16A), CD49d (clone R1-2), CD62L (clone MEL-14), CD44 (clone IM7), 104) (clone A20), CD45.2 (clone 104), CD90.2 (clone 53-2.1), CD107a (clone 1D4B), CD107b (clone M3/84), ARG1 (clone A1exF5, ThermoFisher), GPT2 (clone 16757-1-AP, ThermoFisher), FoxP3 (clone 150D), GR1 (clone RB6-8C5), IL-2 (clone JES6-SH4), IL-4 (clone 11B11), IL-10 (clone JESS-16E3), IL-17A (TC11-18H10.1), IFNg (clone XMG1.2), live/dead near IR (L10119 Thermo Fisher), Ki67 (clone B56, BDbiosciences), Ly6C (clone HK1.4), Ly6G (clone 1A8), pS6 (clone D68F8, Cell Signaling Technology), TCRb (clone H57-597), T-bet (Tbx21, clone 4B10), TNFa (clone MP6-XT22). The influenza PR8-specific NP311-325 tetramer conjugated to BV421 was kindly provided by the NIH tetramer core facility.

Human flow cytometry antibodies/reagents

The following antibodies were used to perform flow cytometry on human cells (all antibodies are from Biolegend unless indicated otherwise): ARG1 (clone 14D2C43), CCR7 (clone G043H7), anti-CD3 (clone RPA-T4), CD4 (clone A161A1), CD8 (clone SK1), CD45RA (clone H1100), CD45RO (clone UCHL1), IFN-γ (clone 4S.B3), IL-10 (clone JES-9D7), IL-4 (clone MP4-25D2), IL-17A (clone BL168), TNFa (Mab11), Ki67 (clone B56, BD biosciences), pSTAT-4 (clone 38, BD Biosciences), pSTAT-1 (clone 4a, BD Biosciences).

Cell surface CAT-1 detection was performed using a soluble ligand derived from the receptor-binding domain (RBD) of the bovine leukemia virus (BLV) envelope glycoprotein (BLV-RBD).[66] Staining was realized with a rabbit Fc-tagged BLV-RBD (BLV.RBD.rabbitIgG1-Fc) (Metafora-biosystems), followed by an anti-rabbit IgG1-Fc secondary antibody (Thermo Fisher), as previously described.[66]

For intracellular staining, BDcytofix/cytoperm buffers were used, except for FOXP3 staining (#00-5523-00, Thermo Fisher) and for pSTAT-1 and pSTAT-4 (# 557870, BD Biosciences phosphoflow fix buffer I and #554656, BD Biosciences phosphoflow perm buffer III) were used according to manufacturer's protocol.

Mouse CD4^{+} T cell isolation and activation

CD4^{+} T cells were isolated from mouse spleens using a negative selection kit according to the manufacturer's protocol (either #130-104-454 from Miltenyi Biotech (Bergisch Gladbach, Germany) or #19852 from Stem Cell Technologies (Vancouver, Canada)). Purity of isolated cells was typically >95%, and cells were resuspended in complete RPMI medium (10% FCS, 2mM glutamine (#25030-149, Gibco), 50U/ml Penicillin + 50μg/ml streptomycin (#15070-063, Gibco) and 2-betamercaptethanol (21985-023, Gibco)). Cells were activated in plates pre-coated with 2ug/ml of anti-CD3 (clone 145-2C11, BioXcell, West Lebanon, NH) at 2x10^{5} per well of a 96 well plate and 5x10^{5} per well of a 48 well plate in the presence of 1ug/ml soluble anti-CD28 (clone 37.51, BioXcell, West Lebanon, NH). After 3 days, the cells were harvest, split into half and seeded into a new plate with 25U/ml Human IL-2 (Peprotech). Cells were harvested and assayed at the indicated timepoints.

Mouse *in vitro* Th1 polarization

Naïve CD4^{+} T cells were isolated from mouse spleens using the manufacturer's protocol (#130-104-453, Miltenyi Biotech). Purity of isolated cells was typically >95%, and cells were resuspended in complete RPMI medium. Cells were plated at 2x10^{5} per well of a 96 well plate and 5x10^{5} per well of a 48 well plate in the presence of feeder cells /antigen presenting cells (irradiated WT splenocytes that were depleted of T cells using a CD3e depletion kit (# 130-094-973, Miltenyi Biotech)), 1μg/ml soluble anti-CD3 (clone 145-2C11, BioXcell, West Lebanon, NH), 20ng/ml of IL-12 (#577004, Biolegend) and 10 μg/ml of anti-IL-4 (clone 11B11, BioXcell, West Lebanon, NH). After 3 days, the cells were harvested, split into half and seeded into a new plate with media containing the same concentrations of IL-12 and anti-IL-4.

Human CD4^{+} T cell isolation and activation

CD4^{+} T cells were isolated from human PBMC or buffy coats after centrifugation using Lymphoprep separation medium (Corning, Vienna, VA) and a negative selection kit according to the manufacturer's protocol (either #130-091-155 from Miltenyi Biotech (Bergisch Gladbach, Germany) or #17952 from Stem Cell Technologies (Vancouver, Canada)). Purity of isolated cells was typically >95%,

Please cite this article in press as: West et al., Loss of CD4+ T cell-intrinsic arginase 1 accelerates Th1 response kinetics and reduces lung pathology during influenza infection, Immunity (2023), https://doi.org/10.1016/j.immuni.2023.07.014

and cells were resuspended in complete RPMI medium (10% FCS, 2mM glutamine (#25030-149, Gibco), 50U/ml Penicillin + 50μg/ml streptomycin (#15070-063, Gibco)). Purified CD4+ T cells were activated for the indicated time points in 96- or 48 well culture plates (Greiner, Monroe, NC) precoated with antibodies to CD3 (clone OKT3) and CD46 (clone TRA2.10)[64] at 1.5-2 x10^5 cells/well (96well) or 3.5-5x10^5/well (48 well) in media containing 50 U/ml recombinant human IL-2 (Peprotech) in an incubator at 37°C and 5% CO_2. Cells were harvested and assayed at the indicated timepoints.

For restimulation experiments, cells were harvested after 36-48 hours of activation and rested for 5 days in 5U/ml recombinant human IL-2 (Peprotech), then harvested, recounted and re-stimulated in plates precoated with CD3 and CD46 antibodies in media containing 50 U/ml recombinant human IL-2 (Peprotech) for 18 hrs.

CD4+ T cell proliferation assessment

Proliferation of *in vitro* activated CD4+ T cells was assessed in two ways. First, isolated Mouse CD4+ T cells were labeled with 2μM cell trace violet (CTV, #C34557, ThermoFisher) according to the manufacturer's protocol. At day 3 post-activation with anti-CD3 and anti-CD28, cells were harvested, stained for CD4 and live/dead and CTV dilution and division index was assessed using a BD Canto (BD biosciences) and FlowJo 10 software (Treestar).

Secondly, *in vitro* activated mouse or human CD4+ T cells were pulsed with 10uM EdU for 2 hours and then harvested and stained for CD4, live/dead and EdU incorporation according to the manufacturers protocol (#C10424 or C10425, ThermoFisher) and were assessed by flow cytometry on a BD FACS CANTO (BD biosciences). EdU was added at the indicated timepoints post-activation.

Cytokine measurements

Cytokine production by *in vitro* activated cells was quantified in cell culture supernatants using human or mouse Th cytokine or Inflammation Legendplex kits (Biolegend) or a mouse IL-10 enhanced sensitivity flex set (BD biosciences) according to the manufacturer's protocol, or by intracellular cytokine staining and flow cytometery after addition of 50ng/ml Phorbol 12-myristate 13-acetate (PMA, #P1585, Sigma Aldrich), 1ug/ml Ionomycin (#13909, Sigma Aldrich) and protein transport inhibitor (#00-4980-03, ThermoFisher) for 4 hours. After 4 hours the cells were harvested, stained for live/dead and CD4 and then fixed and permeabilized (#554714, BD cytofix/cytoperm, BD biosciences, San Diego, CA) and stained intracellularly for cytokines (IFNg, TNFa, IL-17, IL-2, IL-4, IL-10) and assessed by flow cytometry on a BD FACS CANTO (BD biosciences).

Glucose uptake and pS6 evaluation

Glucose uptake: Mouse splenic CD4+ T cells were activated *in vitro* with anti-CD3 and anti-CD28 antibodies. One day post-activation the cells were harvested and washed 2 times with 1x PBS (Gibco). Cells were then seeded into glucose free medium containing 100uM of 2-NBDG (#11046, Cayman Chemicals) or 100uM normal glucose (controls) and were kept in an incubator at 37° C for 2 hours. After 2 hours the cells were washed 2 times with 1x PBS, stained with CD4 and live/dead, washed and assessed by flow cytometry on a BD FACS CANTO (BD biosciences).

Phosphorylated ribosomal S6 protein evaluation: Mouse splenic CD4+ T cells were activated *in vitro* with anti-CD3 and anti-CD28 antibodies. 1 and 3 days post-activation the cells were harvested, washed 2 times, stained with CD4 and live/dead, washed, and fixed and permeabilized. They were then stained with Alexa 647 anti-pS6, washed 3 times and were assessed by flow cytometry on a BD FACS CANTO (BD biosciences).

OCR and ECAR measurements

In vitro stimulated human (anti-CD3 + anti-CD46) or mouse (anti-CD3 + anti-CD28) CD4+ T cells (stimulated for 22-24 hours) were resuspended in serum-free unbuffered Seahorse XF RPMI medium (#103576-100, Agilent Technologies, Santa Clara,CA) that was supplemented with glucose, glutamine and sodium pyruvate. These CD4 T cells were plated onto Cell-Tak (#354241; Corning, Reinach, Switzerland) coated seahorse cell plates at 2.5x10^5 per well. Metabolic profiling was achieved by the perturbation of specific metabolic pathways by the addition of oligomycin (#O4876; 1 μM), Carbonyl cyanide-4-(trifluoromethoxy) phenylhydrazone (FCCP, #C2920; 2 μM) and rotenone (#R8875; 1 μM) +/- Antimycin A (#A8674; 0.5uM) - all from Sigma Aldrich, St. Louis, MO). Metabolic parameters were then calculated based on the following formulas:

(1)basal respiration = [OCR(basal-nc)] – [OCR(rotenone)]
(2) maximal respiratory capacity = [OCR(peak-FCCP)] – [OCR(rotenone)]
(3) spare respiratory capacity =[OCR(peak-FCCP)]-[OCR(basal-nc)]
(4) Basal ECAR= initial rate measured by the extracellular flux analyzer
(5) Maximal ECAR= rate following the addition of rotenone.

Influenza infections, lung cell isolation and virus titers

Influenza infection

6-10 week old mice were infected intranasally (i.n.) with 10^3 EID_{50} of recombinant PR8 influenza virus (expressing the LCMV gp33-41 eptiope (KAVYNFATM) inserted into the NA of A/PR/8/34 (H1N1) (PR8-33) (kindly provided by Dr. Rafi Ahmed (Emory University))[65]

Please cite this article in press as: West et al., Loss of CD4+ T cell-intrinsic arginase 1 accelerates Th1 response kinetics and reduces lung pathology during influenza infection, Immunity (2023), https://doi.org/10.1016/j.immuni.2023.07.014

Lung cell isolation

Lymphocytes were isolated from the lungs as previously described. Briefly, the mice were perfused with PBS, lungs excised, minced and incubated in 1mg/ml Collagenase and 1mg/ml DNase (both from Sigma-Aldrich) in 3ml of RPMI for 45 min at 37 degrees. Single cell suspensions were obtained by pushing the digested lung pieces through a 40uM mesh filter (BD biosciences). Lung lymphocytes were then purified by a 44/67% percoll gradient (Sigma-Aldrich and centrifugation at 2000rpm for 20 min at room temperature.

Lung virus titer assay

After perfusion, one lobe of the lung was excised, weighted, and placed in 1ml of PBS and homogenized using beads and a Minibead Beater (Biospec). They were then cleared by centrifugation and immediately frozen at -80C until needed.

Samples were thawed, serial dilutions performed and placed on a monolayer of MDCK cells (adherent on 96 well plates) for 3 hours at 37° C in the presence of TPCK-trypsin (L-1-tosylamido-2-phenylethyl chloromethyl ketone treated trypsin). The MDCK cells were then washed and DMEM media without trypsin added. 72 hours later, cells were assessed for endpoints in cytopathic effect (CPE). The $TCID_{50}$ titer was then calculated using the Reed-Muench method.[78]

Influenza cytokine assay

This assays was performed as previously described, with some modifications.[5]

Generation of bone marrow derived dendritic cells (BMDCs)

Femurs of B6 CD45.1 mice were placed in 70% ethanol for 2 min to sterilize them and then flushed with cold 1xPBS plus 2% FCS. The cells were then pipetted up and down to break up clumps, washed with PBS, lysed with ACK lysis buffer, washed two times with complete RPMI media and counted. $2x10^6$ bone marrow cells were seeded per 100mM petri dish in 10 ml of complete RPMI media containing 20ng/ml of recombinant mouse Granulocyte-macrophage colony-stimulating factor (rmGM-CSF) and incubated at 37° C for 3 days. On day 3, 10 ml of fresh complete RPMI media containing 20ng/ml rmGM-CSF was added to the plates.

PR8 infection of BMDCs

On day 7 the BMDC cells were harvested, washed with complete media, counted and washed in 1xPBS containing 0.1% BSA. $4x10^6$ BMDCs in 500ul of 1xPBS containing 0.1% BSA were seeded per well into a 6 well plate and 500ul of PR8 influenza virus diluted in PBS containing 0.1% BSA was added per well. The cells were then infected by incubating them for 5 hours at 37° C. After 5 hours the cells were gently scrapped off the plates with cell scrapers, washed 2 times and then kept on ice until co-culture with the lung lymphocytes.

Ex-vivo *assessment of the T cell cytokine response to influenza*

$7.5\ x10^5$ PR8-infected or uninfected (control) BMDCs were mixed with $5.0x10^5$ lung lymphocytes (purified as described above) per well of a 96 well plate in complete RPMI media plus 40U/ml human IL-2 and protein transport inhibitor plus anti-CD107a and CD107b antibodies (or isotypes) for 6 hours at 37° C. After 6 hours, the cells were harvested and stained with live/dead and CD4, CD8, CD90.2 to gate on live lymphocytes and CD45.1 was used to gate out BMDCs. They were then washed, fixed and permeabilized and stained intracellularly for IFNg, IL-2, IL-10 and IL-17A and assessed by flow cytometry.

Influenza Lung Histology

Lungs were excised after PBS perfusion, fixed in 3.7% formalin and embedded in paraffin. 5um sections were cut and stained with hematoxylin and eosin (H&E). Lung pathology scores were based on severity, inflammation, alveoli integrity and bronchi integrity on a graded scale where 0 = normal, 0.5 = very mild, 1 = mild, 2 = moderate, 3 = severe. Samples were blindly scored by a pathologist from the NIH Pathology Core.

$CD4^+$ T cell transfers into *Rag*$^{-/-}$ mice (homeostasis and $CD4^+$ T cell intrinsic influenza experiments).

Homeostasis experiment

Naïve $CD4^+$ T cells were isolated from WT $CD45.1^+$ and *Arg1* CKO ($CD45.2^+$) mouse spleens using the manufacturer's protocol (#130-104-453, Miltenyi Biotech) and combined at a 50:50% ratio (the ratio was assessed by flow cytometry before injection) and $3.2x10^6$ combined cells/mouse were injected i.v. into *Rag1* KO mice. 7 days after cell transfer, the inguinal lymph nodes and spleens were collected.

$CD4^+$ T cell transfer influenza experiment

$CD4^+$ T cells were isolated from WT $CD45.1^+$ and *Arg1* CKO ($CD45.2^+$) mouse spleens using a negative selection kit from Stem Cell Technologies (#19852) according to the manufacturer's protocol. Naïve $CD8^+$ T cells from WT spleens were isolated using a negative selection kit from Miltenyi Biotech (#130-096-543). WT and *Arg1* CKO $CD4^+$ T cell were combined at a 50:50% ratio and then combined with WT naïve $CD8^+$ T cells and injected i.v. into *Rag1* KO mice. 7 days after cell transfer the mice were infected i.n. with PR8-33. 7 days after infection the lungs were perfused and collected for enumeration of cell frequencies.

Colitis induction and colon pathology scoring

Splenic $CD4^+$ T cells were isolated from *Arg1*$^{fl/fl}$ $CD4cre^-$ (WT) and *Arg1*$^{fl/fl}$ $CD4cre^+$ (KO) mice using a negative selection $CD4^+$ T cell isolation kit (Miltenyi Biotech or Stem cell technologies). Cells were stained with anti-CD45RB FITC, anti-CD25 PE and anti-CD4 BV421 and sorted on a SH800S cell sorter (Sony Biotechnology) for $CD4^+$ $CD25^-CD45RB^{hi}$ (brightest 35%) cells. $2.3\ x10^5$ of WT

or KO cells were injected i.p. into age and sex matched C57BL/10 Rag2$^{-/-}$ mice. The mice were sacrificed 6 weeks post adoptive transfer. Spleens and colons were removed, weighted (colons were weighted after flushing out the feces) and colons were measured for length.

Pathology scoring

After flushing the colons of feces, proximal, mid-, and distal colon samples were excised and placed into 3.7% formaldehyde solution, and then paraffin-embedded. Cross-sectional sections were cut and stained with hematoxylin and eosin (H&E). Colon pathology scores were based on severity of mononuclear cell inflammation, intestinal wall thickening, including infiltration to the muscularis, and epithelial damage, including edema, degeneration, and necrosis on a graded scale where 0 = normal, 0.5 = very mild, 1 = mild, 2 = moderate, 3 = severe. Samples were blindly scored by a pathologist from the NIH Pathology Core.

CRISPR-Cas9 deletion of *ARG1*

3 crRNAs were selected using the Benchling online platform (www.benchling.com) and were ordered from Integrated DNA technologies (IDT) in their proprietary Alt-R format: crRNA #1 (sequence GCGCCAAGTCCAGAACCATA) targeting ARG1 exon1; DNA location: chr6:131,573,287-131,573,309. cRNA #2 (sequence chr6:131,581,257-131,581,279) targeting ARG1 exon 4; DNA location chr6:131,581,257-131,581,279. cRNA #3 (sequence GTATATTGGCTTGAGAGACG) targeting ARG1 exon 5; DNA location chr6:131,582,680-131,582,702. 1ul of crRNA and 1ul of tracrRNA (#1072534, IDT reconstituted at 160μM) were mixed in a sterile, RNAse-free PCR tube to create the crRNA-tracrRNA duplexes for each electroporation. Oligos were annealed at 95°C for 5 min in a PCR thermocycler and slowly cooled down to 4°C. Then 1.2μL of Cas9 nuclease (#1081059, IDT) was added to the same tube, and the mixture was incubated 15 min at 37°C to form RNP complexes. The three RNP complexes were pooled and kept on ice until needed.

Up to 10x10^6 of freshly isolated human CD4$^+$ T cells (from healthy donor buffy coats) were used per electroporation. Cells were transferred into 1.5 mL Eppendorf tubes and washed twice with 1x PBS (Gibco) to remove all trace of FCS. Immediately before electroporation, cells were resuspended with 10μL of primary cell nucleofection solution (P3 primary Cell 4D-Nucleofector X kit S (# V4XP-3032, Lonza)), and mixed with RNP complexes and then transferred into electroporation strip. Cells were electroporated using a 4D-nucleofectore core unit (Lonza) and the "EH-100 pulse". Immediately after electroporation, 100 μL of pre-heated cRPMI + 20 UI/mL IL-2 was carefully added directly into each well of the nucleofection strip, and the strip was placed in tissue culture incubator for 15-30 min to allow for cell recovery. Cells were then transferred into a culture plate, resuspended at 2 x 10^6 / mL in cRPMI + 20 UI/mL IL-2 and incubated/rested at 37°C for 3-4 days before stimulation. Cells were then harvested, recounted and re-stimulated in plates precoated with anti-CD3 and CD46 antibodies in media containing 50 U/ml recombinant human IL-2 (Peprotech) for 36hrs. Supernatants were collected to assess overall cytokine secretion and the cells were then assessed by intracellular cytokine staining and flow cytometery after addition of 50ng/ml Phorbol 12-myristate 13-acetate (PMA, Sigma Aldrich), 1ug/ml Ionomycin (Sigma Aldrich) and protein transport inhibitor (#00-4980-03, ThermoFisher) for 4 hours. After 4 hours the cells were harvested, stained with live/dead and CD4 and then fixed and permeabilized (BD cytofix/cytoperm) and stained intracellularly for cytokines (IFN-γ, IL-17, IL-2, IL-10) and assessed by flow cytometry on a BD FACS CANTO (BD biosciences).

ARG1 overexpression

Cells were transferred into 1.5 mL Eppendorf tubes and washed twice with 1x PBS (Gibco) to remove all trace of FCS. Immediately before electroporation, cells were resuspended with 10μL of primary cell nucleofection solution (P3 primary Cell 4D-Nucleofector X kit S (# V4XP-3032, Lonza)), and mixed with 6ug of recombinant ARG-1 (# 71658, BPS Biosciences) and then transferred into an electroporation strip. Control cells were electroporated without ARG-1 protein. Cells were electroporated as above for

CRISPR-Cas9 deletion of *ARG1*, only cells were only rested for 4 hours post-electroporation before being activated with anti-CD3 and anti-CD46 antibodies.

Cell Preparations for Metabolomics

Purified mouse CD4$^+$ T cells were stimulated *in vitro* for 18-22 hours (as indicated in the figure legends) with 2ug/ml of anti-CD3 antibodies coated on plates and 1ug/ml of soluble anti-CD28. Cells were harvested, counted, and washed 2 times with cold PBS, the supernatant aspirated and the cell pellet snap frozen in an ethanol dry ice bath. Cell pellets were kept at -80C or liquid nitrogen until extraction.

For human cells, CD4$^+$ T cells were isolated from PBMC and then washed and processed in the same way as the mouse cells (without *in vitro* activation).

Untargeted Metabolomics

Sample Extraction

Samples were prepared by protein precipitation with cold organic solvent. 800 microliters of ice-cold methanol (Fisher Chemical, Optima™ LC-MS grade) and 200 microliters of water (Fisher Chemical, HPLC grade) were transferred into each 1.5 mL microcentrifuge tube containing a cell pellet. The samples were vortexed briefly (10 s) and placed in a –20°C freezer for 30 min to facilitate precipitation. Samples were subsequently centrifuged for 10 minutes at 14000 relative centrifugal force (rcf) at 4°C (Eppendorf Centrifuge 5425R). 950 microliters of supernatant, referred to as the extract, were transferred into a new 1.5 mL microcentrifuge tube and the pellet was discarded in accordance with chemical and biological safety procedures. The extract was completely dried via

centrifugal evaporation (Genevac EZ-2 Plus) using the HPLC fraction setting and a maximum temperature of 40°C. The dried extracts were capped and stored at -80°C until prepared for analysis.

Sample Resuspension

Dried extracts were removed from storage at -80°C, allowed to warm to room temperature, and resuspended via the addition of 80 microliters of water-acetonitrile 98%:2% v/v. Resuspended extracts were briefly vortexed (15 s). An aliquot from each extract was transferred into a new 1.5 mL microcentrifuge tube to create a pooled quality control sample. An additional aliquot was transferred to a 2 mL autosampler vial with microvolume insert (Agilent).

Analytical Measurement

Samples were analyzed using an ultra-high performance liquid chromatograph (Vanquish, Thermo Scientific) coupled to a high-resolution mass spectrometer (Orbitrap Fusion Tribrid, Thermo Scientific). LC-MS and LC-MS/MS data were acquired. LC-MS data were collected from individual samples (n = 1 injection), system blanks (injection of solvent used to resolubilize samples), and a pooled quality control. The pooled quality control (QC) was injected multiple times at different volumes and used in data processing. LC-MS/MS data, used to annotate features, were collected using the AcquireX (Thermo Scientific) deep scan methodology in which pooled QC was injected multiple times (n = 7). Prior to measurement the mass spectrometer was calibrated using FlexMix (Thermo Scientific) following manufacture directions.

Chromatographic separation was carried out on a 2.1 x 100 mm, 100Å, 2.6 μm, F5 analytical column (Phenomenex) with corresponding guard cartridge. The column was maintained at 30°C during separation with solvent pre-heater. Gradient elution was performed after an initial period of isocratic elution using water with 0.1% acetic acid *v/v* (A) and acetonitrile with 0.1% acetic acid *v/v* (B). Separation was performed as follows: 0% B from 0 - 2.0 min, 0% to 100% B from 2.0 to 10.5 min, 100% B from 10.5 to 12.0 min, 100% to 0% B from 12.0 to 13.0 min, 0% B from 13.0 to 20.0 min. The flow rate was 0.5 mL min^{-1}.

Ionization was performed via heated electrospray ionization (NG Ion Max, Thermo Scientific). The source parameters in positive ionization mode were as follows: spray voltage of +4000 V, sheath gas of 50 arbitrary units (arb), auxiliary gas of 10 arb, sweep gas of 1 arb, ion transfer tube at 325°C, vaporizer at 350 °C. The source parameters used in negative ionization mode were identical except for the spray voltage of -3000 V.

MS and MS/MS data were collected with an anticipated LC peak width of 8 s and a default charge of 1. EASY-IC™ (Thermo Scientific) was installed and used during data collection; a lock-mass is measured, concurrently to experimental measurement, and used for instrument mass calibration. MS data were acquired at 120,000 resolution from *m/z* 100-1000 with an RF lens of 60% and maximum injection time of 50 ms. MS/MS data were acquired at 30,000 resolution using an isolation width of 1.5 (*m/z*), stepped assisted HCD (energy steps were 20, 35, and 60, and a maximum injection time of 54 ms. The inclusion list was generated and updated via AcquireX with a low and high mass tolerance of 5 ppm. An intensity filter was applied via the ''Intensity'' node in the workflow with an intensity threshold of 2.0e4. The ''Dynamic Exclusion'' node was used with the following parameters: exclude after n = 3 times, if occurs within 15 s, exclusion duration of 6 s, a low mass tolerance of 5 ppm, a high mass tolerance of 5 ppm, and excluding isotopes.

Untargeted Metabolomics Data Processing

Compound Discoverer 3.3.0.550 (Thermo Scientific) was used to process.raw files which resulted in a tabular output which included descriptors of each feature (*e.g. m/z*, retention time), annotation information (*e.g.* MS/MS database match), and peak area. We processed the output from Compound Discoverer using in-house R scripts via JupyterNotebooks. The major components of the processing included formatting of the data outputs, comparison of *m/z* and retention time of annotation features versus an in-house generated list based on authentic chemical standards, assessment of signal response in pooled QC samples, assessment of signal variance in pooled QC samples versus samples (*i.e.* dispersion ratio), and multi- and univariate statistics. MSI levels of annotation confidence[79] were provided based on the MS/MS database matching algorithm in Compound Discoverer, a list of *m/z* generated from authentic chemical standards, and manual annotation. All features with a MS/MS database match remained at level 2 while those matching the *m/z* and retention time criteria were promoted to level 1.

Glutamine, and glutamic acid were searched for in the processed and cleaned dataset. We affirmed the annotation of glutamine (318|130.04985|0.446) in the positive ion mode and glutamic acid (100|146.04608|0.443) in the negative ion mode to level 1 confidence based on MS/MS matching, *m/z* mass error, and retention time similarity to authentic chemical standard (Figure S7).

Extraction of hydrophilic metabolites for amino acid and polyamine measurement

To extract hydrophilic molecules an adapted three-phase solvent system was utilized to separate hydrophilic metabolites from lipids, proteins, and nucleic acids.[80] Briefly, the cell pellets were resuspended in 0.15 mL of ice-col saline and then 1.2 mL of chloroform/methanol/water (3:4:1, v/v/v) was added. Next, the tube homogenized using a Bead Ruptor Elite (OMNI international, Kennesaw GA, USA) for 30 sec at 8 m/s. The homogenate was allowed to rest on ice for 30 sec and then centrifuged for 15 min at 21,000 g at 4°C. After centrifugation, the upper aqueous phases were transferred into new tubes, frozen on dry-ice and then dried by lyophilization.

Mouse amino acid and polyamine measurement

Dried extracts containing the hydrophilic metabolites were dissolved in 30 μl of water/acetonitrile (8:2, v/v) and 10 μl were used in the procedure to derivatize amino acids as described previously[81] with some modifications. In brief, the samples were placed into a glass autosampler vials and then 35 μl of sodium borate buffer (100 mM, pH 9.0) was added and mixed by pipetting. Next, 10 μl of the 6-aminoquinolyl-N-hydroxysuccinimidyl carbamate (AQC, 10 mM in acetonitrile)-derivatizing reagent (Cayman Chemical) was

added. The vial was sealed, mixed by vortexing, and then incubated at 55°C for 15 min. The vial was cooled to room temperature and then 15 μL were analyzed by liquid chromatography coupled to mass spectrometry (LC-MS/MS). A Vanquish Horizon UHPLC (Thermo Fisher Scientific, Waltham, MA, USA) was used for the LC separations, using a linear gradient conditions as follows: 0–0.5 min 2% B; 0.5–1.5 min 2 to 96% B; 1.5–2.5 min 96% B; 2.5–3.5 min 96 to 2% B; 3.5–5 min 2% B. Mobile phase A was water/acetonitrile (97:3, v/v) supplemented with 10 mM ammonium acetate and 10 mM ammonium hydroxide. Mobile phase B was acetonitrile. The column used was an Accucore C30 (250 x 2.1 mm, 2.6 μm) (Thermo Fisher Scientific, Waltham, MA, USA), operated at 45 °C. The flow rate was 300 μL/min and the injection volume used was 15 μL. All LC/MS solvents and reagents were the highest purity available (water, acetonitrile, ammonium acetate, ammonium hydroxide) purchased from Thermo Fisher Scientific (Waltham, MA, USA). A Thermo Scientific Q Exactive hybrid quadrupole-Orbitrap mass spectrometer (QE-MS) (Thermo Fisher Scientific, Waltham, MA, USA) equipped with a HESI-II probe was employed as detector. The QE-MS was operated in the negative ion mode using a targeted selected ion monitoring followed by a data-dependent MS/MS method (tSIM/dd-MS^2). The QE-MS was operated at a resolution of 140,000 (FWHM, at m/z 200), AGC targeted of $1x10^6$, Max injection time 80 msec. For the dd-MS^2 conditions a resolution of 35,000 was used, AGC targeted of $1x10^5$, Max injection time 40 msec, MS^2 isolation width 0.5 m/z and NCE 35. The source's operating conditions were: Sheath gas flow 45, Aux gas flow 8, Sweep gas 1, Spray voltage 2.6 kV in negative ion mode, Capillary temp 325°C, S-lenses RF level 55, Aux gas heater 325 °C. The monitored parent/daughter ions and the retention-time windows for each amino acid is listed in Table S5. The acquired tSIM data was processed using the software application Skyline 21.2 (MacCoss Lab Software).

GC-MS-mediated analysis of TCA metabolites and ^{13}C-labelled TCA metabolites

The method applied was based on procedure previously published by Zhang J. et al.[82] Briefly, cells were stimulated *in vitro* for 12-16 hours (with anti-CD3 + anti-CD28 (mouse) or anti-CD3 + anti-CD46 (human)). Cells were then harvested, washed 2 times with glutamine free medium, counted and incubated in glutamine-free RPMI medium (10% FBS, penicillin/streptomycin) supplemented with 2mM of standard glutamine or [U-^{13}C]-glutamine (Cambridge Isotope Laboratories, Inc.) for 6 hours. Next, cells were collected, washed with ice-cold saline solution, snap-frozen and stored in liquid nitrogen for further processing. Extraction of hydrophilic metabolites was performed using 2x volume of methanol/water solution (2:1 v/v, HPLC-grade, with added 5nM of norvaline as internal standard). Next, samples were homogenized and mixed with 1 volume of chlorophorm (HPLC-grade). Subsequently, derivatization with 2% methoxylamine-HCl solution and GC-MS-grade MTBSTFA + 1% t-BDMCS reagent was performed as reported by Zhang et al.[82] Samples were analyzed in split-less mode using Agilent 7890B GC system equipped with a 5977B MSD, Agilent VF5ms, +1m EZ, 60m, 0.25, 0.25 μM column, helium carrier gas and Mass Hunter software package. Chromatographic gradient conditions: separation time 36 min; start at 80°C, 1 min; ramp to 250°C at 7°C/min; ramp to 300°C at 50°C/min and hold for 9 min. MSD settings: source 150°C; quadrupole 150°C; interface 300°C; injector 250°C; EI source 70 eV, EI pressure 1.8×10^{-5} torr. Signals were acquired under SIM mode conditions according to Zhang et al. as well as in scan mode (full scan range 50-500 m/z at ~ 2 scans/s (N=3)).[82] Enrichment in C^{13}-labelled isotopomers was corrected by their natural abundance using "standard glutamine" medium-incubated sample as reference and Mass Hunter software.

Human polyamine measurement

Measurement of polyamines was performed using the p180 targeted quantification kit (Biocrates) in the Duke Proteomics and Metabolomics Shared Resource. Briefly, sample extraction was performed by adding 30 uL of 3:1 v/v methanol chloroform to the samples, followed by probe sonication 3 bursts of 5 seconds each with cooling on ice between. Samples were spun at 15000 rpm for 10 minutes, and 15 uL of the clear supernatant was added to the Biocrates p180 extraction plate. Subsequent extraction, derivatization and analysis by LC-MS/MS was performed according to manufacturer protocol on a Waters TQ-XS mass spectrometer.

RNAseq Library preparation and analysis

Total RNA was isolated from splenic $CD4^+$ T cells harvested after 24hr of *in vitro* activation or influenza infection, or lung $CD11a^+CD49d^+TCRb^+$ $CD4^+$ T cells sorted (BD FACS aria, San Diego, CA) from influenza-infected mice using, using an RNAqueous Micro Kit (Cat# AM1931, source: Invitrogen). After DNAse I digestion, RNA was subjected to library preparation using poly(A) mRNA capture (catalog# E7770 and E7490, source: NEB) according to manufacturer's protocol. Libraries were sequenced on a Novaseq Illumina platform. After fastqc check samples were mapped and aligned using bowtie2[67] and RSubread/v 2.8.1[68] to the mm10 genome, respectively. The mapping criteria for bowtie2 was: "–sensitive-local –no-unal" where indexes used were generated using UCSC/mm10 genome. Subsequently all libraries from these samples were normalized (as RPKM) and mRNAs expression and list of DEGs was calculated using EdgeR/v 3.36.0[69] tools using the following criteria: at least $\log_2$ 4-fold change in either direction at FDR < 0.05, after removing genes with minimal expression. Pathways enriched in DEGs were calculated using the Molecular Signatures Database v.7.5.1[72] accessed at url https://www.gsea-msigdb.org/gsea/msigdb/annotate.jsp. Heatmaps were drawn using Morpheus from the Broad Institute (https://software.broadinstitute.org/morpheus) and visualized using DataGraph v 5.0 (Visual Data Tools, Inc.) and Adobe® Illustrator 2021.

Microarray preparation and analysis

All scripts and data to replicate the microarray analysis are available at https://github.com/jackbibby1/E-West and data are deposited at GEO at GSE 229775. Total $CD4^+$ T cells of two patients with Arginase 1-deficiency and two age – and sex-matched healthy

controls were isolated using CD4+ T cell positive selection beads (Miltenyi Biotech) and activated for 6 hours *in vitro* with immobilized antibodies to CD3 and CD46, both at 2ug/ml, in the presence of 25U/ml IL-2. Total RNA was isolated and gene array analyses performed using the Illumina chip HT-12v4 Expression BeadChip (Illumina, San Diego, CA, USA).

Raw data were processed and analyzed using limma,[71] which involved filtering using detection P Values and normalization using neqc. Normalized data were then used as an input to Gene Set Enrichment Analysis.[70] Parameters used for GSEA were as follows: permutations = 1000, permutation type = gene set, enrichment statistic = weighted, ranking metric = ratio of classes, min/max gene set size = 15/500. Data visualization was done using ggplot2.[83]

QUANTIFICATION AND STATISTICAL ANALYSIS

Figures 1A, 1G, 2A, 3A, 3E, 3I, 4A, and 4H and the graphical abstract were created with BioRender.com. Analyses were performed using GraphPad PRISM 9.4.1 (La Jolla, CA, USA). Data are presented as mean ± SD or median (interquartile range, IQR) for parametric and non-parametric data, respectively, and compared using (two-tailed paired and unpaired) *t*-tests, Wilcoxon signed rank tests, the (two-tailed) Mann-Whitney test, one-way ANOVA, or the Kruskall-Wallis test as appropriate. p values < 0.05 are denoted statistically significant throughout. All experiments were carried out in at least triplicate technical and biological replicates unless otherwise stated. Gene set enrichment analyses (GSEA) of RNA-sequencing data utilized in this study were performed using GSEA version 3.0.[70]